

Pontificia Universidad Católica del Perú

Escuela de Posgrado



Orbital Angular Momentum in an driven Optical Parametric
Oscillator

A thesis in candidacy for the degree of Master of Science in Physics

Author:

Junior Ricardo Gonzales Ureta

Advisors:

Carlos Eduardo Rodrigues de Souza (UFF)

Francisco Antonio de Zela Martinez (PUCP)

March 2018

Resumen

El control del Momento Angular Orbital (OAM por sus siglas en inglés) de la luz en sistemas óptico cuánticos puede proveernos de un grado adicional de libertad, lo cual nos puede permitir muchas aplicaciones en mecánica cuántica y tecnologías de la comunicación que tengan como eje central la óptica en su desarrollo. Luz laser con OAM, vórtices ópticos, son generalmente descritos por modos de Laguerre-Gaussianos, los cuales tienen una distribución de intensidad tipo dona, con singularidades de fase en su frente de onda. En este caso particular los modos son de primer orden y la esfera de Poincaré da una conveniente representación geométrica para el subespacio expandido por esta base. Continuando la propuesta teórica hecha por B. Coutinho dos Santos et al. en 2007 [1], en este proyecto estamos interesados en estudiar de forma experimental la dinámica de un Oscilador Paramétrico Óptico (OPO) bajo la inyección de un haz con OAM. El objetivo principal es caracterizar la conservación de OAM en los haces gemelos, nombrados "signal" y "idler" por razones históricas, provenientes del OPO inyectado, de acuerdo a una simetría no trivial en la esfera de Poincaré. Otro objetivo es el estudio teórico de la dinámica de los haces de luz gemelos, de acuerdo a parámetros experimentales reales del arreglo usado, y de ese modo mejorar la eficiencia en la creación de los fotones gemelos, lo cual permitiría el estudio experimental del entrelazamiento cuántico con este aparato. También, en la mira de este trabajo se encuentra, la medición y caracterización del "squeezing" que fue realizada en el recientemente montado OPO de la UFF.

Abstract

The control of the Orbital Angular Momentum (OAM) of light in quantum optical system can provide an additional degree of freedom, that can enable many applications in quantum mechanics and optical communications. Lasers beams with OAM (optical vortices) are generally described by Laguerre-Gaussian modes, which have a doughnut intensity distribution with phase singularities in the wavefront . In the special case of first order OAM modes, the Poincaré sphere gives a convenient geometrical representation of those optical vortices . Following the theoretical proposal done by B.Coutinho dos Santos et. al in 2007 [1], in this project we are interested in studying experimentally the dynamics of an Optical Parametric Oscillator under the injection of a seed beam with OAM. The main aim of this project is to characterize the OAM conservation in the twin beams, namely signal and idler, coming from the injected Optical Parametric Oscillator, according to the symmetry in the Poincaré sphere. We aim also at studying theoretically the dynamics of the twin beams generated, according to the real experimental parameters of the setup, to improve the twin beams creation efficiency, which will enable us to study experimentally quantum entanglement in this apparatus. Also, in the scope of this work, the measurements and characterization of squeezing was performed in the recent mounted OPO at UFF.

Acknowledgments

First of all I would like to thank God for keeping me alive and healthy , and making me able to finish this work on time , even when I know it is not usual that scientist have such believes , whatever that means , I feel that many circumstances on my life could be attributed to luck , but I like to think that there is a direction on what I do , even when I can not give a proof of this.

I have also to say thanks to my colleagues, that joined me on the this travel to Brazil, that in one way or another help me not only on the academic part but also in the living regards. Thanks to all my teacher that help me to get here, since the school, the academy and the university, specially to Prof. Francisco de Zela for giving me the opportunity to start working on the quantum optics laboratory on Lima. In this place I learn with effort the basics techniques employed on the lab regarding to interferometry, thanks to Omar Ortiz , Yonny Yugra ,Diego Barberena and Piero Sanchez for being patient while teaching me and the enlightening discussions on the daily work.

I could not be able to develop this work without the help of the Peruvian government that gave me a scholarship through CONCYTEC that supports my master studies as well as my living cost, and the PUCP that also provided important contribution along my academic life, and I hope keep doing it.

Thanks to all the people that I met on the UFF , specially to the quantum optics lab team there, they taught me the very basics on the cavity and OAM manipulation, topics that were completely new for me, and I was very glad to be able to learn and also collaborate with. Thanks to professor A.Z Khoury for accepting us, a group of young students in his lab, and also for the patience during the classes, and his absolute confidence to answer any question even the crazier ones.

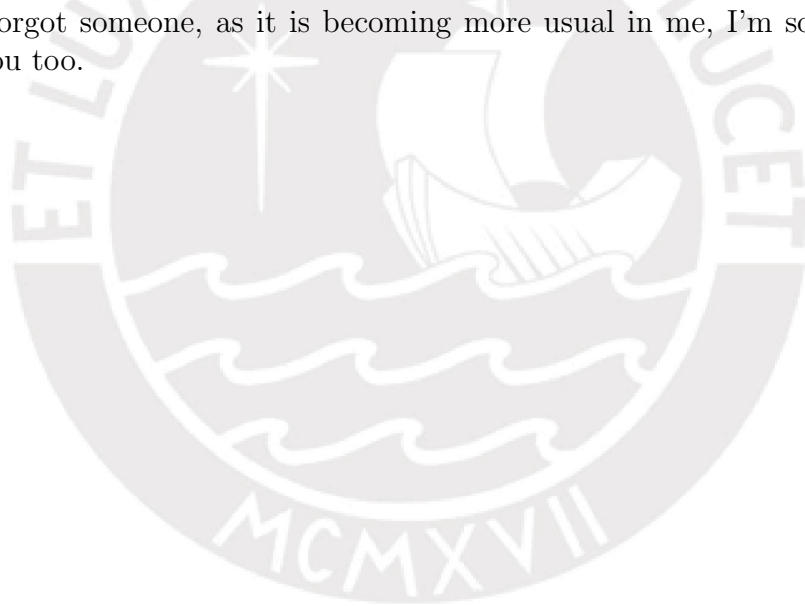
A special shout-out to professor Carlos Eduardo Rodrigues de Souza, not only for the enormous help given to me while learning all the nuances of the work in optical resonators, but also for all the post-internship advice and

enlightening reviews on the writing of my thesis. I would like to emphasize the excellent person that he is, as well as Rafael Bellas, great people that I had the pleasure to meet and work daily on the UFF, treating me as a long time friend, something that I really appreciated.

I must also thank to my family and friends that are here, and all the ones that have already passed away, that always worry for me, call me and send their best regard even when I'm in the other side of the world. Thanks to my father that supports me through my whole physics studies , even when I know he disagrees with my chosen career , but he still keeps supporting me, so I think he finally accepted it.

Finally , probably the only one that believes more in me than even myself, Sabina my mom, she was, is and will be my main motivation to keep going on, keep moving forward , and to make her proud of me is probably the greatest feeling I have ever had. That is why I never give up and never will.

If I forgot someone, as it is becoming more usual in me, I'm sorry, but thank you too.



Contents

Resumen	i
Abstract	ii
Acknowledgments	iii
1 Introduction	1
2 Theoretical Background	3
2.1 Paraxial Wave Approximation	3
2.2 Transverse Spatial Modes	4
2.2.1 Hermite Gaussian Modes	4
2.2.2 Laguerre Gaussian Modes	5
2.3 Polarization	9
2.4 Orbital Angular Momentum (OAM)	9
2.5 First Order Poincare Sphere	11
3 Optical Cavities or Resonators	15
3.1 ABCD Law	15
3.2 Stability	18
3.3 Resonant Frequencies	21
3.4 Losses in Optical Resonators	23
4 Experimental Procedures	24
4.1 Mode Matching	24
4.2 Characterization	25
4.3 Manipulation	26
4.4 Tilted Lens Method	28
4.5 Pound Drever Hall Method	29

5	Quantum Correlations of Light	32
5.1	Entanglement	32
5.2	Parametric Down Conversion	34
6	Optical Parametric Oscillator	36
6.1	Non-linear Susceptibility	36
6.2	Subtraction of Frequencies	38
6.3	Dynamic Equations	39
6.4	Stationary Solutions	41
6.5	Stability	43
6.6	Numerical Simulation	46
7	Squeezing	50
7.1	Coherent States	50
7.2	Generalized Quadratures	51
7.3	Experimental Results	54
7.4	Conclusions	57
8	Injected Optical Parametric Oscillator	58
8.1	Free Running OPO	59
8.2	Injected OPO Dynamics	61
8.3	Experimental Proposal	62
8.4	Experimental Results	64
8.5	Conclusions	66
9	Summary and Conclusions	69

Chapter 1

Introduction

The present work is based on the dynamics of optical cavities with the presence of beams carrying OAM. This is important, due to the ongoing developments in quantum information science and quantum information technology. These new approaches to the information transmission and communications are strongly based on the quantum mechanical principles of the individual particles or systems.

Quantum mechanics, which was born in the 20th Century, is in some sense a recent theory, as compared to Newtonian mechanics or thermodynamics. As I like to emphasize, quantum mechanics is more than just a theory created to explain certain experiments in the early 1920's. Quantum mechanics is rather a framework, because nowadays it is almost impossible to avoid taking into account its principles in any new theoretical proposal, because quantum predictions have been confirmed by almost any experiment. The interpretation and philosophical implication are still kind of blurry in the mind of many but that is something secondary in the path of quantum information developments.

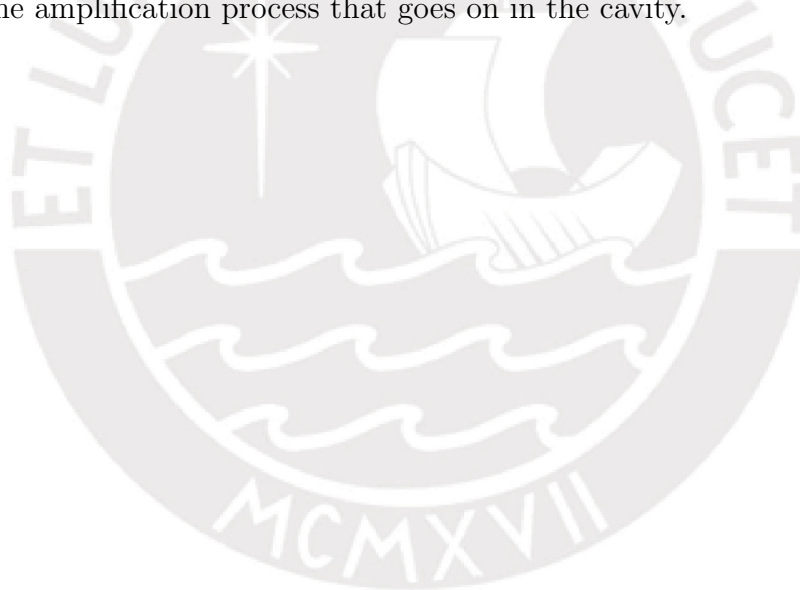
Perhaps a huge step in the technological revolution was done 55 years ago [2] with the development of the laser, which led people to perform experiments that could seem very counterintuitive at first sight. Fundamental experiments that reveal features about superposition or nonlocality which nowadays are said as day-to-day things were confirmed thanks to these developments, and constituted one essential step further in quantum communications, quantum teleportation, quantum cryptography and quantum computation.

Most of these fields use qubits (2 level systems), due to the complexity of

creating higher dimensional systems. Here is when the OAM shows a great advantage over other quantities used before by other systems (polarization, momentum, spin). In principle, the OAM is a discrete quantity (1) that can be exhibited by photons and classical beams (lasers) that have a field distribution in the form of Laguerre-Gaussian modes, which do not have an upper bound.

The study of OAM could help to develop new protocols to encode information with increased capacity due to the high dimensions that can be achieved. Also, because it is an electromagnetic field property encoded in light, it can be transmitted over long distances.

The work performed here, even if it was done with only qubits as the first approximation, could well scale up into higher dimensional bits (qudits), being robust under decoherence due to the fact that the output beams are created in a quantum mechanical regime, but reach macroscopic intensities due to the amplification process that goes on in the cavity.



Chapter 2

Theoretical Background

For the sake of completeness, we reproduce here some well-known results that could be found even at the level of textbooks [3] [4] [5]. However, we will not dwell on presenting detailed calculations, but focus on those results concerning, e.g., the intensity distribution across the transverse section of a laser beam and the like, which are connected with our main concern, namely those features which are related to the OAM.

2.1 Paraxial Wave Approximation

It is important to mention that in the most general case the whole phenomena of electromagnetism rely on the Maxwell equations that we all know. However, for our purposes, we can limit ourselves to deal with the paraxial approximation.

If we do not consider the time dependence of an electromagnetic wave nor its vectorial character for the moment, and only focus on the spatial distribution of intensity, we can write its amplitude as:

$$A(x, y, z) = a(x, y, z)e^{ikz} \quad (2.1)$$

The amplitude function (A) of the field will depend on (x, y, z), but we will consider only beams propagating along the z -direction. Here is when the paraxial approximation comes in handy, if we assume that the beam does not change its amplitude considerably within a range of propagation of the order of the wavelength. This means that $\Delta a \ll a$. We can consider the complex exponential as a field being modulated by “ a ” (called spatial mode). Taking

these considerations into account and inserting them into the classical wave equation deduced from Maxwell theory, we get the paraxial wave equation (PWE)

$$(\nabla_{\perp}^2 + ikz \frac{\partial}{\partial z})a(x, y, z) = 0 \quad (2.2)$$

Here the ∇_{\perp} means the Laplacian operator over the coordinates on the transverse plane. These coordinates could be Cartesian coordinates or any other ones. This feature will be what brings us to the study of different spatial modes.

2.2 Transverse Spatial Modes

In this section we show the results of solving the PWE in two coordinate systems, Cartesian and cylindrical. The family of modes that emerges from these two systems is the one that we use in our experiment.

2.2.1 Hermite Gaussian Modes

This type of modes arises from the solutions of the PWE in Cartesian coordinates [6], and has the form:

$$HG_{n,m}(x, y, z) = CHG_{n,m} \frac{1}{\omega(z)} H_n\left(\frac{\sqrt{2}x}{\omega(z)}\right) H_m\left(\frac{\sqrt{2}y}{\omega(z)}\right) \exp\left(\frac{ik(x^2 + y^2)}{2R(z)}\right) \exp\left(\frac{-(x^2 + y^2)}{\omega^2(z)}\right) \exp(i\phi_{m,n}) \quad (2.3)$$

with the normalization constant

$$CHG_{n,m} = \frac{\sqrt{2}}{\sqrt{\pi m! n! 2^{m+n}}} \quad (2.4)$$

The meanings of the parameters are as follows:

$\omega(z)$ is the beam diameter that depends on the position along the propagation axis, in this case the z-axis. It is given by:

$$\omega(z) = \omega_0 \sqrt{1 + \left(\frac{z}{z_r}\right)^2} \quad (2.5)$$

where ω_0 is the beam diameter at its narrowest point. z_r is known as the Rayleigh length, and is given by:

$$z_r = \frac{\pi\omega_0^2}{\lambda} \quad (2.6)$$

$R(z)$ Is the radius of curvature of the mode, and is given by :

$$R(z) = z \left(1 + \left(\frac{z_r^2}{z^2} \right) \right) \quad (2.7)$$

It is worth to mention that it tells us that only when the beam is at the origin or at infinity ($z = 0$ or $z = \infty$), the radius will be infinite, which means the wavefront is a plane. $\phi_{m,n}$ is called the Gouy phase, and is given by:

$$\phi_{m,n} = \left(1 + \frac{m+n}{2} \right) \arctan \left(\frac{z}{z_r} \right) \quad (2.8)$$

Finally, what gives these modes their name and characterize the intensity distribution, are the Hermite polynomials:

$$H_n = (-1)^n \exp(x^2) \frac{d^n}{dx^n} \exp(-x^2) \quad (2.9)$$

For the sake of clarity and to get a feeling for this kind of beams, we plot the intensity distribution and check the implications of the indexes, n and m, written above, in Figure 2.1

2.2.2 Laguerre Gaussian Modes

The next mode will be a consequence of solving the PWE with cylindrical coordinates. They are described by:

$$\begin{aligned} LG_{n,m}(r, \theta, z) = & CLG_{n,m} \frac{1}{\omega(z)} \exp \left(\frac{-r^2}{\omega(z)^2} \right) \exp \left(\frac{-ikr^2}{2R(z)} \right) \\ & \exp(-i(n+m+1) \arctan \left(\frac{z}{z_r} \right)) \exp(-i(n-m)\theta) \\ & (-1)^{\min(n,m)} \left(\frac{r\sqrt{2}}{\omega(z)} \right)^{|n-m|} L_{\min(n,m)}^{|n-m|} \left(\frac{2r^2}{\omega(z)^2} \right) \end{aligned} \quad (2.10)$$

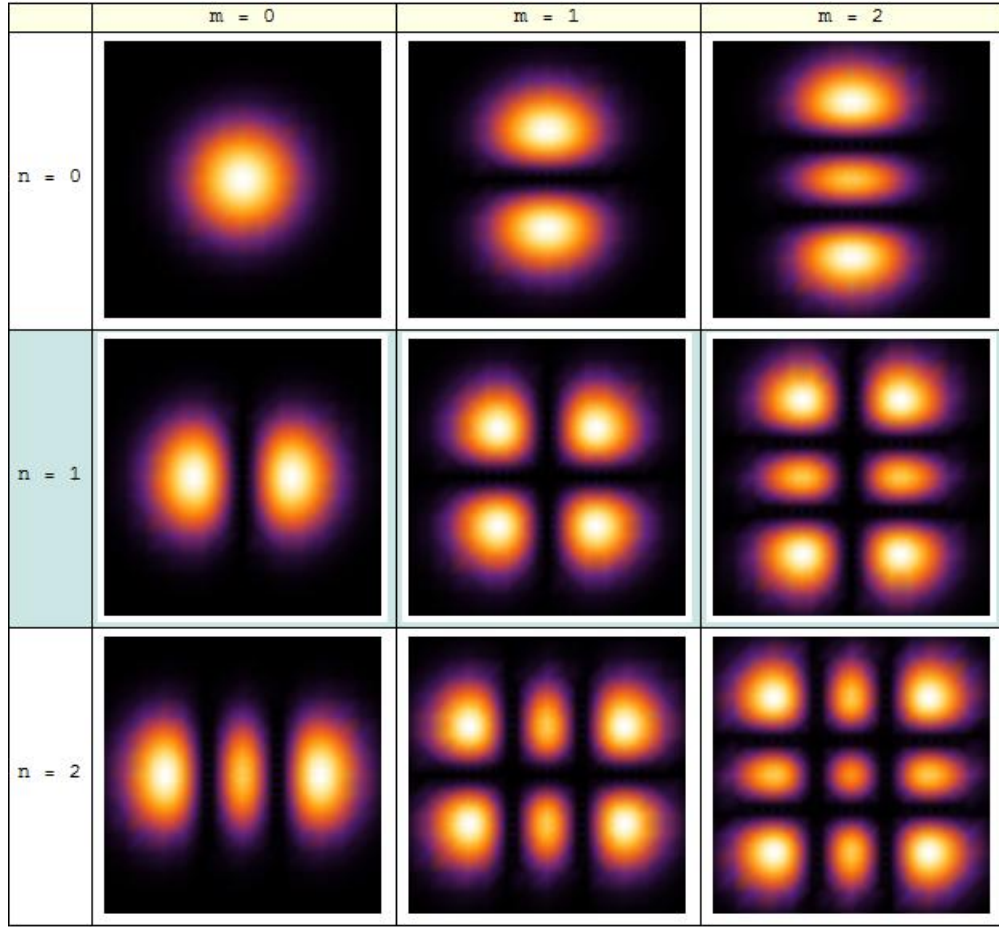


Figure 2.1: As we can see here in the table, the index n give us the number of vertical nodal lines (null intensity) of the beam, while the index m the horizontal ones.

with normalization constant

$$CLG_{n,m} = \left(\frac{2}{\pi n! m!} \right)^{\frac{1}{2}} \min(n, m) \quad (2.11)$$

Most of the parameters have already being explained. However, this is not the most common way to write the expression for the Laguerre – Gaussian beams, but this notation will be useful when we try to show the link with the Hermite- Gaussian beams later on. It is easy to come up with the standard way to write the Laguerre – Gaussian beams with the replacement:

$$\begin{aligned} l &= m - n \\ \rho &= \min(n, m) \end{aligned} \quad (2.12)$$

Even though it could seem confusing at first sight, the usage of these two new indexes will prove to be very instructive to label the Laguerre beams as follows:

$$\begin{aligned} LG_{\rho,l}(r, \theta, z) &= \frac{\sqrt{2\rho!}}{\sqrt{\pi(|l| + \rho)!}} \left(\frac{\sqrt{2}r}{\omega(z)} \right)^{|l|} \frac{1}{\omega(z)} \exp\left(\frac{-r^2}{\omega(z)^2}\right) \exp\left(\frac{-ikr^2}{2R(z)}\right) \\ &\quad \exp(-i(|l| + \rho + 1) \arctan\left(\frac{z}{z_r}\right)) \exp(-il\theta) L_{\rho}^{|l|}\left(\frac{2r^2}{\omega(z)^2}\right) \end{aligned} \quad (2.13)$$

where $L_{\rho}^{|l|}$ are the Laguerre polynomials :

$$L_{\rho}^l(r) = e^r \frac{r^{-l}}{\rho!} \frac{d^{\rho}}{dr^{\rho}} (e^{-r} r^{\rho+l}) \quad (2.14)$$

It is also worth to single out the term $e^{il\theta}$, which tells us that the phase distribution of the wavefront has an angular dependence, giving rise to a helical phase structure of the wavefront along the propagation axis. Due to it, there will be a phase singularity at the origin of the beam.

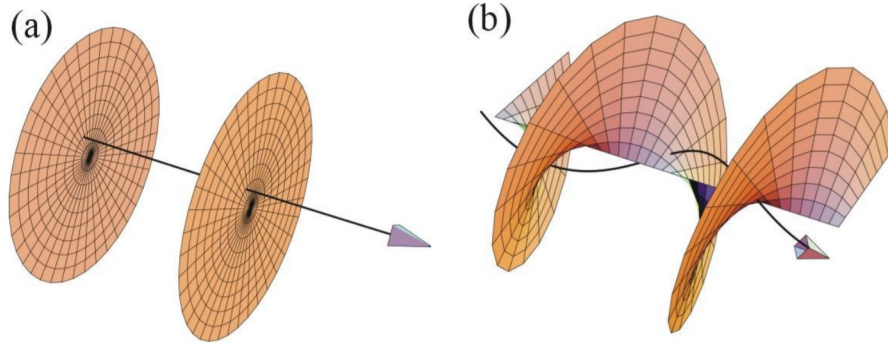


Figure 2.2: a) shows a plane wavefront, while b) shows a helical wavefront corresponding to a wave carrying OAM

The number of times that the helix will achieve a complete twist within a wavelength will be determined by l , while the sign of l will set the sense of

the twist (clockwise or counterclockwise). The parameter l is also known as topological charge, and plays a major role in the following discussion about Orbital Angular Momentum. The reason to add ρ to label the states of the Laguerre beams can be seen in Figure 2.3.

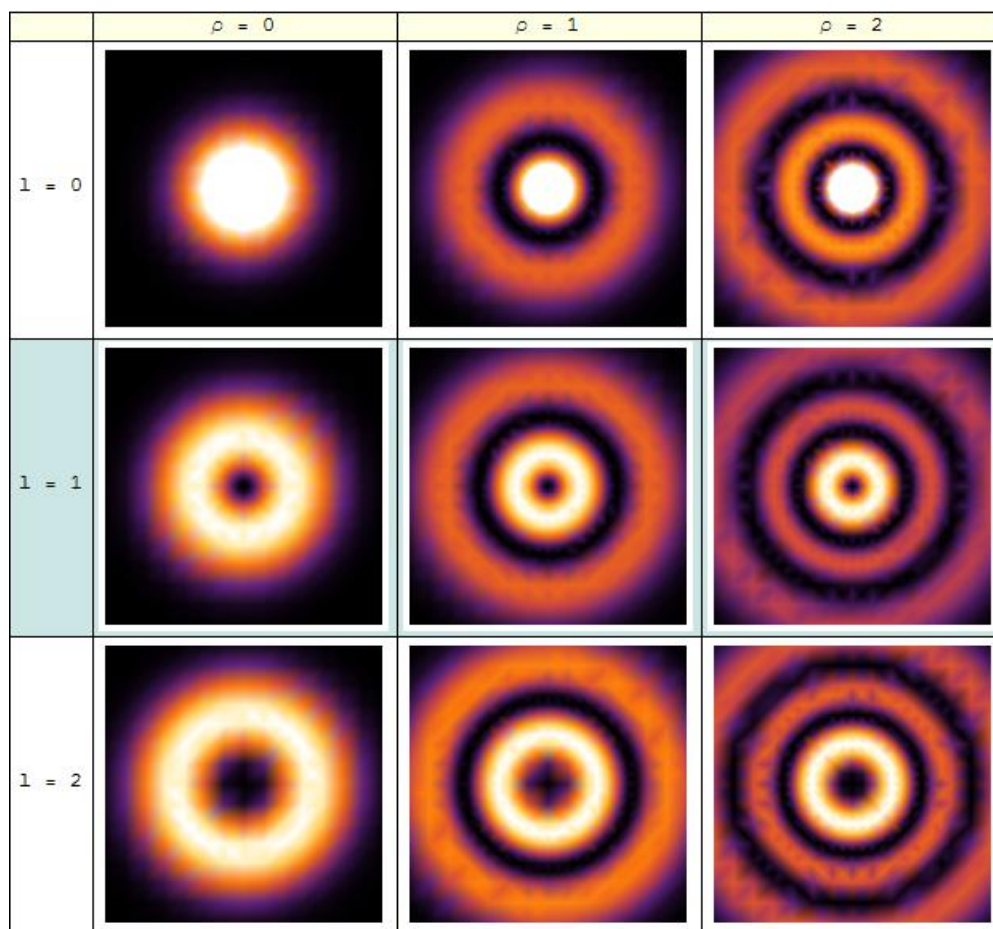


Figure 2.3: Here we can see that makes a lot of sense the standard way to write the Laguerre beams, the index ρ give us the number of radial nodal lines, while the topological charge the number of twist of the wavefront, of course this is not visible in intensity plots, as the ones shown in this table

2.3 Polarization

Up to this point, we have ignored completely the vectorial nature of light, because we were mainly dealing with intensity distributions (scalar). However, we should keep in mind that Maxwell equations are vectorial ones.

The polarization of a beam is contained in the transverse plane, so it is a bi-dimensional vector space. We can choose two orthonormal vectors to be used as a basis, and depending on the relative phase between them different kinds of polarization will emerge. To exemplify, let us write our basis and assume a relative phase difference δ , choosing Cartesian coordinates only for simplicity.

$$\begin{aligned}\vec{e}_h &= Ae^{i\omega t}\vec{x} \\ \vec{e}_v &= Be^{i\omega t+\delta}\vec{y}\end{aligned}\tag{2.15}$$

The polarization of any beam will be composed by the sum $\vec{e}_T = \vec{e}_h + \vec{e}_v$, and we can see in Figure 2.4 that different cases arise:

In our experiments, we have used mainly linearly polarized light in the whole beam. It also deserves attention the case of so-called vector beams. They show a more complex structure due to the fact that not only their intensity and phase distribution change across the transverse plane, but also the polarization at each point. Much research is ongoing, concerning these topics, but it lies beyond the scope of this work.

2.4 Orbital Angular Momentum (OAM)

The standard definition of total angular momentum derived from classical electrodynamics is [7]

$$J = \int \epsilon_0 \mu_0 \vec{r} \times (\vec{E} \times \vec{H}) dV.\tag{2.16}$$

Using the identity $\mu_0 \vec{H} = \nabla \times \vec{A}$ and Gauss' theorem, we can re-write the total angular momentum as:

$$\vec{J} = \int \epsilon_0 E_i (\vec{r} \times \nabla) A_i dV + \int \epsilon_0 \vec{E} \times \vec{A} dV\tag{2.17}$$

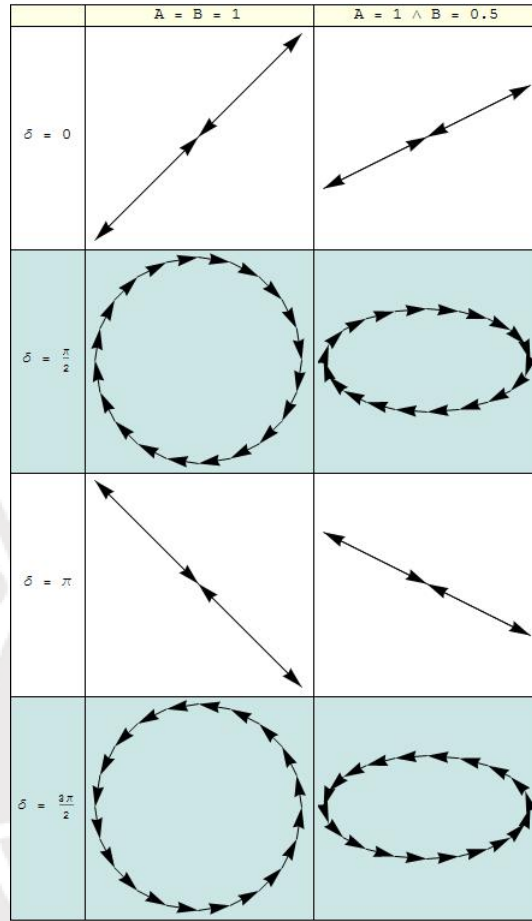


Figure 2.4: We will call the cases of equal amplitude: diagonal, left circular, anti-diagonal and right circular polarization in the same order as presented in the table, all of them arise from different relative phases. Let's keep in mind that the electric field oscillates over time, always relative to an origin, in the case of linear polarizations it's pretty clear, but the left and right circular polarized is the direction that follows the circle plotted above. For completeness the second column shows the case where both amplitudes are different, as can be seen elliptical polarization appears. We must mention that when the A or B are zero, we have vertical and horizontal polarization respectively.

Where the separation in two parts has clear purposes: the first term of the sum depends on the coordinate system, while the second one is independent of it. Let us realize that the second term will never vanish unless \vec{A} or \vec{E} are

zero, so in that sense we can recognize it as the intrinsic part of the angular momentum. While the first term has a dependence on the reference system.

Checking this features, and in analogy to quantum mechanics we can recognize the first term as the orbital part of the angular momentum, while the second one as the spin part of the angular momentum, and write :

$$\hat{J} = \hat{L} + \hat{S} \quad (2.18)$$

Here, we still need to remember that \hat{J} is the physical quantity that should be conserved over time, not \hat{L} or \hat{S} , because it is what emerges from symmetry of rotation in our Lagrangian, or the operator that commutes with the Hamiltonian $[\hat{H}, \hat{J}]$, depending on what formalism is required, or more handy to deal with.

Here we are going to be supported by important developments done related to the OAM, mainly by Allen and Woerdmann [8], who showed that it is possible to assign a definite discrete value of OAM to beams with a helical phase structure (i.e. $e^{il\theta}$), depending on the number of twists within a wavelength (l). This important fact makes it possible to connect the OAM with the Laguerre - Gaussian modes studied before. What we called “topological charge” quantifies the OAM that our beam carries, playing a major role in the experiments that will be detailed later on.

Finally, I would like to mention that it is also possible that a beam carries fractional values of OAM, even though it was beyond the scope of the experiments we have performed, it could be an interesting topic to move on in later research.

2.5 First Order Poincare Sphere

First let us take a look at the polarization system. As already said, it is a two-dimensional vector space. We defined the orthonormal basis (\hat{e}_h, \hat{e}_v) , and it was shown that depending on their amplitudes and relative phase we can reach different kinds of polarization. It could also be seen as if this two-dimensional vector space was defined over a complex field. It brings us to an important way to present polarization states, widely used in polarimetric experiments: the Poincare Sphere (Figure 2.5).

We are going to deal only with first order Laguerre modes, so it would be useful to have a representation for them, in a similar fashion to the one used for polarization. The order of a beam is given by $N = n + m$ for both

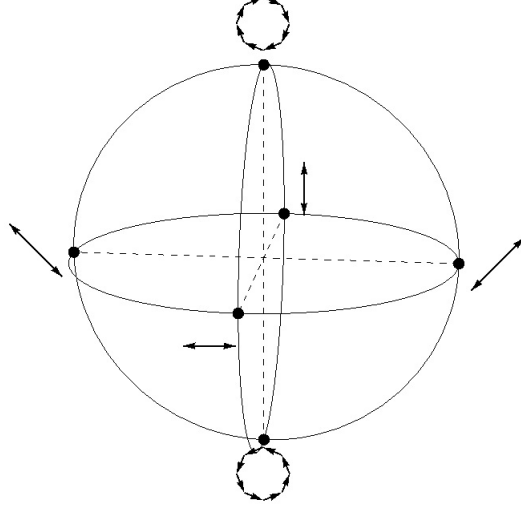


Figure 2.5: Here is the so called Poincare Sphere, that has in the equator the linear polarizations, any linear combination of horizontal and vertical polarization with real coefficients, while at the north pole the left circular polarization (clockwise), and at the bottom the Right circular polarization (counterclockwise)

families of modes, but in the standard notation used for Laguerre modes it will be $N = |l| + 2\rho$.

Following the steps described above for the polarization case, we would need to pick an orthonormal basis. Using a natural definition for an internal product in a functional space, as :

$$\langle f(x)|g(x)\rangle = \int_{-\infty}^{+\infty} f(x)g(x) dx \quad (2.19)$$

Where we can show using the Hermite polynomial identities that:

$$\langle HG_{n,m}|HG_{n',m'}\rangle = \delta_{m,m'}\delta_{n,n'} \quad (2.20)$$

As M.W. Beijersbergen [9] pointed out, a Laguerre mode can be written in terms of Hermite modes of the same order.

$$LG_{n,m}(x, y, z) = \sum_{k=0}^N i^k b(n, m, k) HG_{N-k,k}(x, y, z) \quad (2.21)$$

with real coefficients

$$b(n, m, k) = \left(\frac{(N-k)!k!}{2^N n!m!} \right)^{\frac{1}{2}} \times \frac{1}{k!} \frac{d^k}{dt^k} [(1-t)^n (1+t)^m] |_{t=0} \quad (2.22)$$

Where the i^k corresponds to a phase difference of $\frac{\pi}{2}$ between successive modes.

Also with the same coefficients, a Hermite-Gaussian mode that has a nodal line rotated 45° , can be decomposed as:

$$HG_{n,m} \left(\frac{x+y}{\sqrt{2}}, \frac{x-y}{\sqrt{2}}, z \right) = \sum_{k=0}^N b(n, m, k) HG_{N-k,k}(x, y, z) \quad (2.23)$$

with all the HG modes in the sum being in phase between one another. As these powerful results hold on for any index m and n , we can easily construct our two-level OAM sphere for modes of order 1, with $HG_{1,0}$ and $HG_{0,1}$ as the basis, in analogy to \hat{e}_h and \hat{e}_v . So we would have in similar fashion a representation in a sphere (see Figure 2.6)

From this point on, we move on to Chapter 3, in which we will basically describe the operating principle of the optical resonators, which constitute the basic structure of the OPO used in this work.

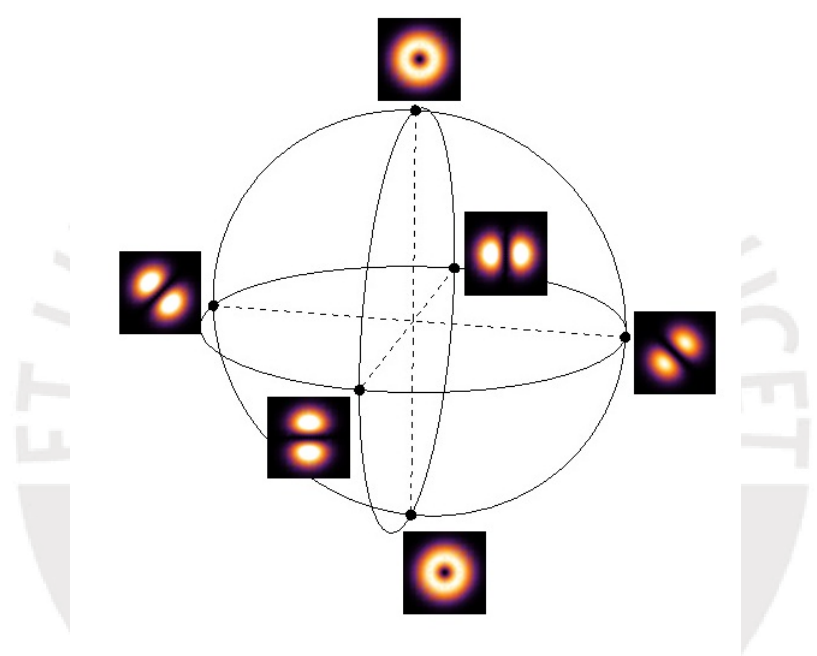


Figure 2.6: Here is the representation analogous to the Poincare Sphere, this time for OAM, there the first order Hermite modes, serve as the horizontal and vertical polarization, in the equator are all linear combination of them with real coefficients, at the north pole there the Laguerre mode with topological charge +1, in the south the one carrying -1 , of course its impossible to recognize this phase information on intensity plots.

Chapter 3

Optical Cavities or Resonators

In our experiment, the optical resonators were used for two purposes. The first one is to filter the noise coming from the laser, and the second one is to amplify the intensity inside the cavity. In that way we can amplify the non-linear process) generated by the Non linear crystal that we are going to talk about later on. In the following discussion we will take certain tools to analyze what happens inside the resonator and its output behavior. Most of the content of this chapter is based on the text book of Amnon Yariv, “Quantum Electronics” [10]

3.1 ABCD Law

It is important to first analyze the propagation of an optical ray through many optical devices, especially through lenses and spherical mirrors

To achieve it, we are going to describe an optical ray by two parameters r and $r' = \frac{dr}{dz}$ assuming the z -axis as the propagation axis. They represent the distance to the axis of propagation and its slope, respectively.

We would like to see how some optical devices transform these two parameters. Let us start by the most common instrument in an optics laboratory: a lens, and to simplify calculus, a thin lens, which is a very usual assumption while working on the paraxial regime.

As can be seen from the Figure 3.1 and using the ray method, the new

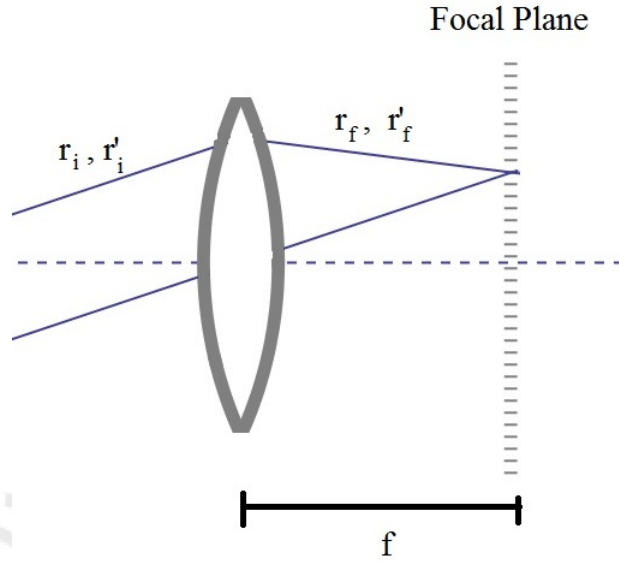


Figure 3.1: The deflection of a ray incident from the left side, as we are dealing with the thin lens the position doesn't change and using classical ray traces we can determine the new slope.

parameters are:

$$\begin{aligned} r_f &= r_i \\ r'_f &= r'_i - \frac{r_i}{f} \end{aligned} \quad (3.1)$$

Of course we can enforce (eq.3.1) to be written in a more compact way if we build a vector $(r, r')^t$, so that the transformation can be seen as a matrix operating over our new vector.

$$\begin{pmatrix} r_f \\ r'_f \end{pmatrix} = \begin{pmatrix} 1 & 0 \\ -\frac{1}{f} & 1 \end{pmatrix} \begin{pmatrix} r_i \\ r'_i \end{pmatrix} \quad (3.2)$$

using the usual conventions in optics, $f > 0$ for a converging lens and $f < 0$ for a diverging one.

By the same token, we can construct the matrices that represent other optical devices, in particular we are interested in the spherical mirrors, lenses (already commented) and of course the propagation in a homogeneous medium.

As you can see in Figure 3.2

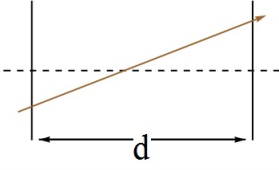
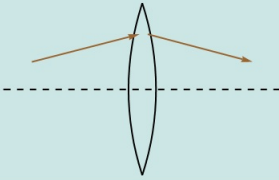
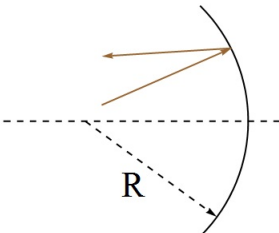
Element	Representation (r,r')	Physical Situation
Homogeneous Medium	$\begin{pmatrix} 1 & d \\ 0 & 1 \end{pmatrix}$	
Thin Lens	$\begin{pmatrix} 1 & 0 \\ -\frac{1}{f} & 1 \end{pmatrix}$	
Spherical Mirror	$\begin{pmatrix} 1 & 0 \\ -\frac{2}{R} & 1 \end{pmatrix}$	

Figure 3.2: Here we see the proper matrices that will be very useful in the following discussion, and a ray representation of changes performed by these 3 optical elements, all these matrices can be inferred by the snell law, and physical consideration

3.2 Stability

With these tool we can study the dynamics of an optical ray inside a cavity, we are going to consider a simple resonator, i.e., light confined between two spherical mirrors. It can also be applied to plane mirrors $R \rightarrow \infty$, with a length d . Schematically we are going to perform:

$$\begin{pmatrix} r_{i+1} \\ r'_{i+1} \end{pmatrix} = M_{mirror}(R_2) \cdot M_{space}(d) \cdot M_{mirror}(R_1) \cdot M_{space}(d) \cdot \begin{pmatrix} r_i \\ r'_i \end{pmatrix} \quad (3.3)$$

Using the specific matrices, the above expression yields:

$$\begin{pmatrix} r_{i+1} \\ r'_{i+1} \end{pmatrix} = \begin{pmatrix} 1 - \frac{2d}{R_1} & d \left(2 - \frac{2d}{R_1} \right) \\ \frac{-2(-2d+R_1+R_2)}{R_1 R_2} & \frac{4d^2 + R_1 R_2 - 2d(2R_1 + R_2)}{R_1 R_2} \end{pmatrix} \cdot \begin{pmatrix} r_i \\ r'_i \end{pmatrix} \quad (3.4)$$

Here $(r_{i+1}, r'_{i+1})^t$ means the state after a round trip inside the cavity, from eq.3.4

$$r'_i = \frac{1}{d \left(2 - \frac{2d}{R_1} \right)} \left(r_{i+1} - \left(1 - \frac{2d}{R_1} \right) r_i \right) \quad (3.5)$$

Of course, eq. 3.4 and eq.3.5 are valid for the second round trip $(r_{i+2}, r'_{i+2})^t$, so we can write:

$$r'_{i+1} = \frac{1}{d \left(2 - \frac{2d}{R_1} \right)} \left(r_{i+2} - \left(1 - \frac{2d}{R_1} \right) r_{i+1} \right) \quad (3.6)$$

Using eq. 3.4 and eq. 3.6, we get an important equation:

$$r_{i+2} - 2br_{i+1} + r_i = 0 \quad (3.7)$$

With

$$b = 1 - \frac{2d}{R_1} - \frac{2d}{R_2} + \frac{2d^2}{R_1 R_2} \quad (3.8)$$

We can see equation 3.7 in analogy to the differential equation $r'' + Ar = 0$, which helps us to get some guide about the solutions. That brings us to try the very useful “ansatz” or educated guess $r_i = Ae^{ij\alpha}$, using j as the imaginary unit, just to avoid confusions, it leads us to:

$$e^{2j\alpha} - 2be^{j\alpha} + 1 = 0 \quad (3.9)$$

Solving eq. 3.9 as a quadratic equation for $e^{j\alpha}$, we get:

$$e^{j\alpha} = b \pm j\sqrt{1-b^2} \quad (3.10)$$

Taking linear combinations of the ansatz, we can reach the general solution

$$\begin{aligned} r_i &= r_{max} \sin i\alpha + \delta \\ r_{max} &= \frac{r_0}{\sin \delta} \\ \tan \delta &= \frac{r_0 \alpha}{dr'_0} \end{aligned} \quad (3.11)$$

Here is clear that $\cos \alpha = b$, if and only if $b^2 \leq 1$. This is going to be our criteria to judge if a ray beam is confined to a region, in this case the resonator. We want the angle $\alpha \in \mathbb{R}$, otherwise the parameter r would keep growing, and at some point the ray will escape. It also imposes the following condition over b :

$$-1 \leq b \leq 1 \quad (3.12)$$

Going back to the parameters of our resonator, eq. 3.8 reads:

$$-1 \leq 1 - \frac{2d}{R_1} - \frac{2d}{R_2} + \frac{2d^2}{R_1 R_2} \leq 1 \quad (3.13)$$

If we divide the expression by 2, add $\frac{1}{2}$, and factorizing we get the usual way to write the stability condition for a resonator made by two spherical mirrors:

$$0 \leq \left(1 - \frac{d}{R_1}\right) \left(1 - \frac{d}{R_2}\right) \leq 1 \quad (3.14)$$

Now we can trace the rays inside the cavity, specifying their coordinates in a Cartesian system. The X and Y points are independent (see Herriot et al. [11]), so they emerge in the same form as the solutions of equation 3.11 and we can write them like:

$$\begin{aligned} x_m &= x_{max} \sin n\alpha + \delta_x \\ y_m &= y_{max} \sin n\alpha + \delta_y \end{aligned} \quad (3.15)$$

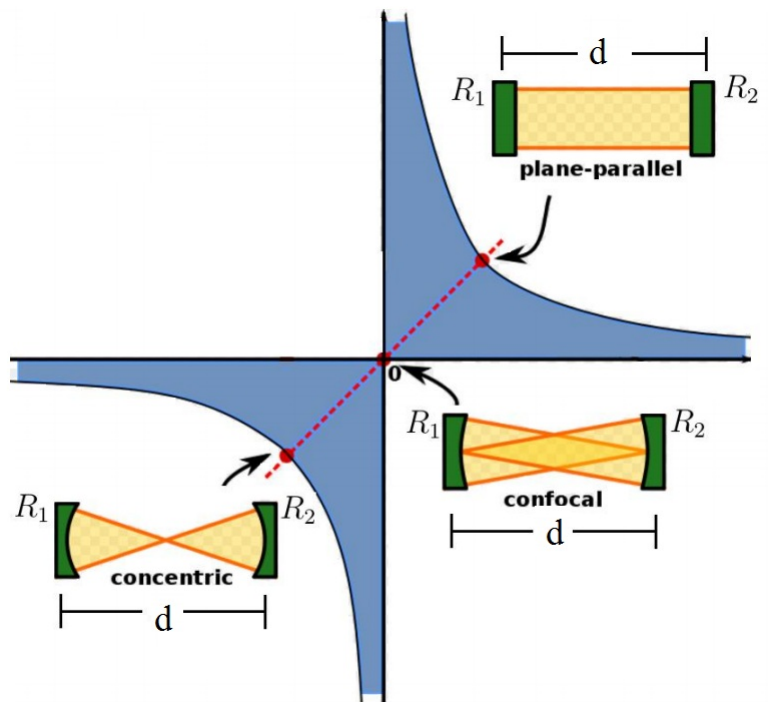


Figure 3.3: Here are shown some cavity configurations, that will be discussed latter, but as we can see they operate in the limit of estability (region blue is the stability zone according to eq. 3.14) so any deviation from the ideal parameters will disrupt the functioning

Here n refers to the number of reflections on the cavity suffered by the beam, and the parameter α is given by:

$$\alpha = \frac{2l\pi}{\nu} \quad (3.16)$$

with l and ν that taking any integer values, they tell us that our beam will come back to the starting point after ν round trips. It means that the ray is confined inside the cavity of course, because after a finite number of reflections it will draw a closed curve (do not forget that all rays are straight lines). We can check the above result by applying it to some simple cases; see Figure 3.4

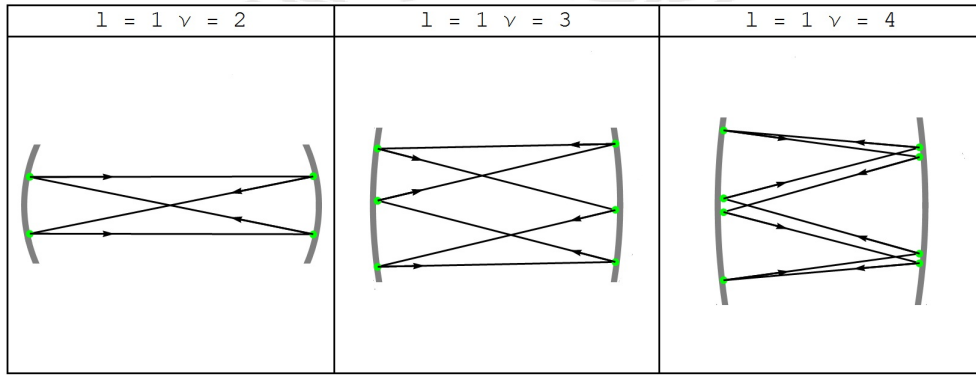


Figure 3.4: Here we see a table that plots the index mention at 3.16, the gray surfaces are the spherical mirrors and the green points the reflections, the index ν enumerates the number of round trips that the ray need to come back to the starting point, of course it's only possible because we respect the stability condition, otherwise the rays will escape the cavity

3.3 Resonant Frequencies

Now we need to analyze the conditions necessary for the formation of standing waves inside the cavity in terms of phase or space. Both aspects are analogous. We can formulate the conditions in terms of the beam's frequency or the cavity length. Following the discussion in "Quantum Electronics" by Yariv [10] we are going to express these relations in frequency, but in the proper experiment we did not have control over it. We changed the cavity length to scan the resonances of the system.

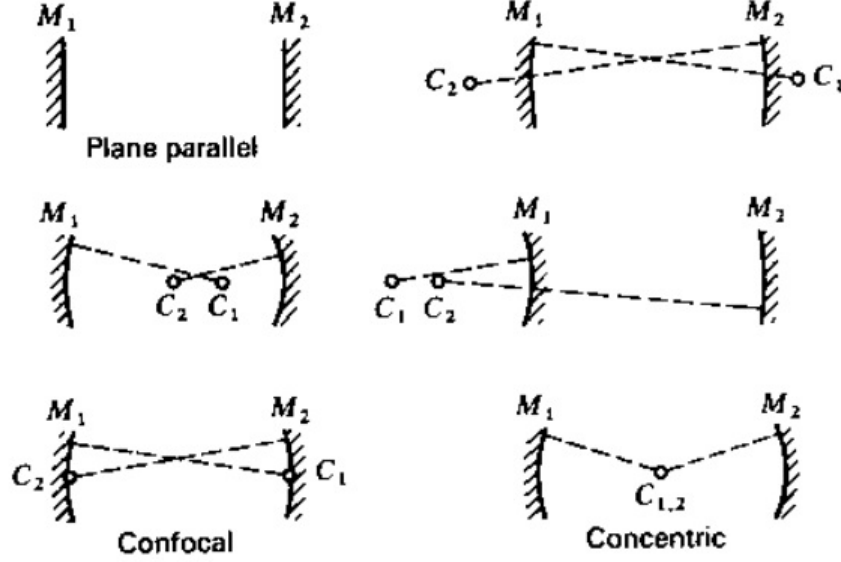


Figure 3.5: : Here some examples of configurations with different kind of mirror are shown. This figure is taken from “Quantum Electronics” by Yariv.

The resonance’s condition is expressed in terms of the Gouy phase, see equation 2.8, for our cavity with boundary conditions (mirrors) at z_1 and z_2 and the phase that arises from the direction of propagation e^{ikz} :

$$\phi_{m,n}(z_2) - \phi_{m,n}(z_1) = q\pi \quad (3.17)$$

Here we defined $l = z_2 - z_1$ to get:

$$kl - (m + n + 1) \left(\arctan \left(\frac{z_2}{z_0} \right) - \arctan \left(\frac{z_1}{z_0} \right) \right) = q\pi \quad (3.18)$$

Now let us check the case of two fields of different orders (this analysis will later prove to be useful). Equation 3.18 holds for any beam order, so that:

$$\begin{aligned} k_1 l - (m + n + 1)_1 \left(\arctan \left(\frac{z_2}{z_0} \right) - \arctan \left(\frac{z_1}{z_0} \right) \right) &= q\pi \\ k_2 l - (m + n + 1)_2 \left(\arctan \left(\frac{z_2}{z_0} \right) - \arctan \left(\frac{z_1}{z_0} \right) \right) &= q\pi \end{aligned} \quad (3.19)$$

Subtracting the equations in 3.19 and using $k_1 - k_2 = \frac{2\Delta\nu}{c}$, we obtain:

$$\Delta\nu = \frac{c}{2\pi l} \Delta(m+n) \left(\arctan\left(\frac{z_2}{z_0}\right) - \arctan\left(\frac{z_1}{z_0}\right) \right) \quad (3.20)$$

This expression is crucial for our purposes, it tells us that the resonance frequency depends on the order of the mode we are inserting, or thinking in terms of length, the position of the resonance peaks will differ from order to order.

3.4 Losses in Optical Resonators

An important parameter used for quantifying how good an optical cavity is, is the so called “Quality Factor” (Q), defined by :

$$Q = \frac{\omega E}{P} = \frac{\omega E}{dE/dt} \quad (3.21)$$

Here E means the energy contained in the cavity, and P the dissipated power. Many models can be proposed to explain the obvious power dissipation in real cavities. Pointed by Born and Wolf [3], in his textbook, the Q-factor relates to the spectral separation of the resonance frequencies, and can be written as

$$\Delta\nu = \frac{\nu}{Q} \quad (3.22)$$

which could be easily assessed if we know the frequency of the field inside the cavity (ν), and we check the output signal through a oscilloscope.

Chapter 4

Experimental Procedures

In this section I will discuss many procedures that usually are not mentioned in publications, or textbooks. However, they are fundamental to make that the experiments actually work. All these techniques were taught to me by the laboratory team at UFF. I thus dispense myself

4.1 Mode Matching

Optical cavities are very sensible to any misalignment, including those related to the wavefront radius of curvature. Here the waist $\omega(z)$ and the radius of curvature $R(z)$ play a major role, because as it is obvious any optical cavity will have reflective surfaces (usually mirrors) as frontiers to enforce the light to be most confined.

We achieve the mode matching condition when the form of our wavefront matches perfectly with the geometry of the reflective surface, because otherwise no matter how reflective is our surface, the light will start to experiment successive reflections that will throw it outside the axis of the cavity, reducing its efficiency.

As we can imagine, it is not always possible to create a cavity of an arbitrary length due to the fact that the mirrors (usually spherical) available have fixed radius of curvature, or for any other practical reason we need a certain length of the cavity. So we require two things, first of all characterize the beam we are working with, it means to determine the ω_0 , and, second, change this parameters to our requirements to achieve the mode matching condition $R_{beam}(z_{mirror}) = R_{mirror}$.

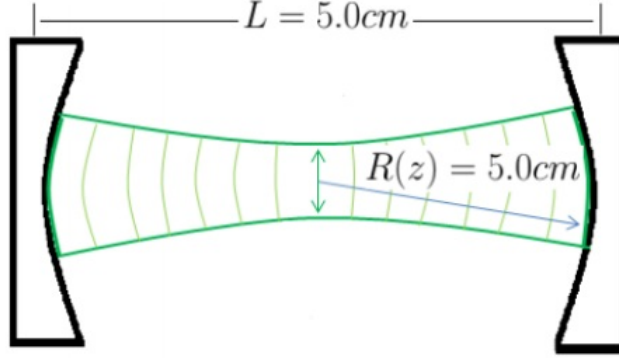


Figure 4.1: Example of a typical wavefront inside a cavity, it will not be plane, so the radius curvature at the mirror must match, “Mode Matching”

4.2 Characterization

Let us start with a given beam, of ω_0 unknown. What we are allowed to assume is that the beam must follow the equation 2.5, so we would like to make an appropriate number of measurements and then fit a curve that will help us to get the value ω_0 and its relative position. In our case, we can only perform intensity measurements. What we did was to take advantage of the radial symmetry that the fundamental and Laguerre modes exhibit. We can partially block the beam at two specific points, first at $x_{n,1} = -\frac{\omega(z_n)}{2}$ and then at $x_{n,2} = \frac{\omega(z_n)}{2}$. The beam diameter at an arbitrary point z_n will be given by the difference $x_{n,2} - x_{n,1} = \omega(z_n)$. The above procedure may seem to be circular, because we are trying to get $\omega(z)$ by intensity measurements at points that depend on it. However, if we integrate the module of equation 2.3, which is normalized over the whole plane $x - y$, for $m = n = 0$ (fundamental Gaussian mode), we get:

$$\begin{aligned} \int_{-\infty}^{+\infty} \int_{-\infty}^{x_{n,1}} |HG_{0,0}|^2 dx dy &\approx 0.8413 \\ \int_{-\infty}^{+\infty} \int_{-\infty}^{x_{n,2}} |HG_{0,0}|^2 dx dy &\approx 0.1586 \end{aligned} \quad (4.1)$$

As we can see, these values are fractions of the total intensity (normalized to 1), independent of the value and position of the waist. In practice it means

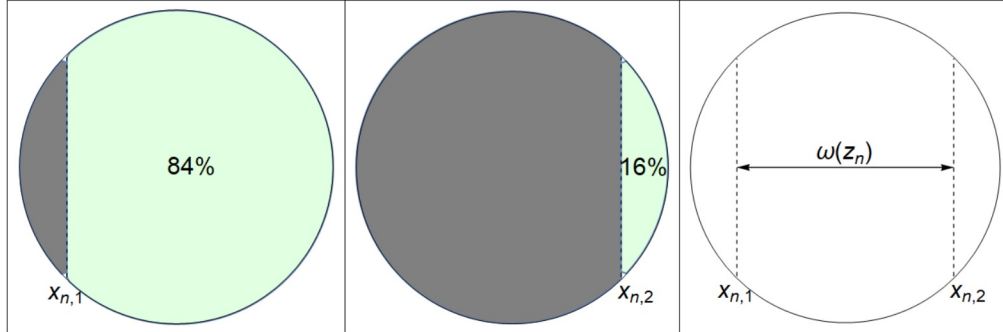


Figure 4.2: Here the pictures are representations of the transverse section of the beam, the green area is what the powermeter would measure, the gray area is the beam section blocked, also the percentages of the whole intensity are shown at each step. The last image shows the effective diameter of the Gaussian beam, its important to make emphasis when we say “effective”, because the equations 2.3 and 2.10 never imply a limit in the intensity distribution, they can be consider to expand over the whole transverse plane of course with smaller values when they get further away from the origin. In practice is needed a limit, to work with. This sequence of measurements are done along the axis of propagation to be able to generate a sensible fit.

that we can mount a beam stopper over a micrometrical displacer and move it until we measure approximately 84 % of the total intensity, save the position, and then repeat it to get 16 %, then subtract both positions and obtain a value for the point $\omega(z_n)$. Repeating this procedure an appropriate number of times, we can fit the data to equation 2.5.

It is important to mention that for a Laguerre mode the intensities will differ from 84% and 16 %, due to their different radial distribution of intensity, but the new values can be calculated in the same way.

4.3 Manipulation

We are interested in changing the value of ω_0 , for this we use the formalism of “ABCD” matrices,also called “ray transfer matrix analysis”, that tells us the way optical devices change the propagation of beam rays. Let us define the “complex beam parameter” $q(z)$:

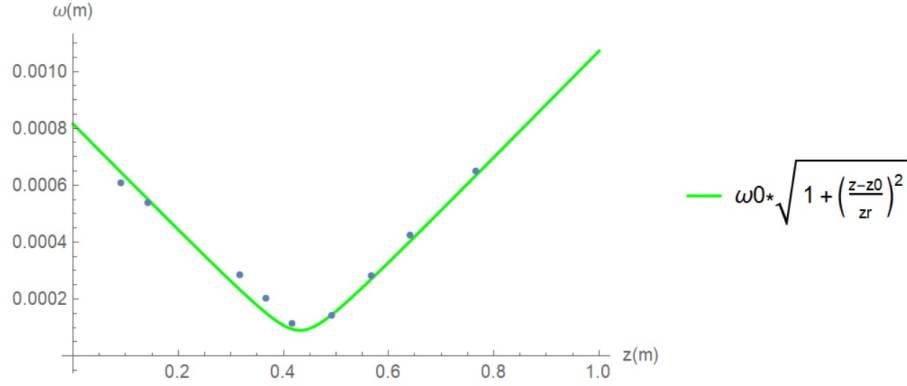


Figure 4.3: This is one the many characterizations done at the lab during the experiment. Here the blue points are experimental data, recorder as was described before, and the green curve is the fit done with Mathematica, it gave us values for the waist $\omega_0 = 90.10 \pm 2.6\mu\text{m}$ and the distance to it $z_0 = 0.43 \pm 0.006\text{m}$. The last parameter appears due to the fact that at the beginning of the measurements we pick an arbitrary origin for z .

$$\frac{1}{q(z)} = \frac{1}{R(z)} - \frac{i\lambda_0}{\pi n\omega(z)^2} \quad (4.2)$$

Here n does not refer to any mode label (we are still talking about the fundamental mode), it refers to the refraction index of the medium where the light is traveling. It also can be reformulated as:

$$q(z) = z + iz_r \quad (4.3)$$

here z is the distance to ω_0 , and z_r the Rayleigh length. Given an initial complex parameter q_0 we can use the ray transfer matrix of our optical system and compute the resulting q_f .

$$M_{opt\text{ syst}} = \begin{pmatrix} A & B \\ C & D \end{pmatrix} \quad (4.4)$$

$$q_f = \frac{Aq_0 + B}{Cq_0 + D}$$

The new q_f will tell us the new value for the waist and its position. In these experiments, we will use lenses to get the required waist value. The transferred ray matrix needed are:

$$\begin{aligned}
M_{lens} &= \begin{pmatrix} 1 & 0 \\ -\frac{1}{f} & 1 \end{pmatrix} \\
M_{free} &= \begin{pmatrix} 1 & d \\ 0 & 1 \end{pmatrix} \\
M_{system} &= M_{lens} \cdot M_{free}
\end{aligned} \tag{4.5}$$

Where f is the lens focal length, and d refers to the distance that the beams travel in free space. As in any formalism that works with non commutative elements, the order is important. We are implying that our beams first go through the lens, and then propagate. Our resulting complex parameter following 4.4 and 4.5 reads:

$$q_f = \frac{f \times (q + d)}{f - d - q} \tag{4.6}$$

Usually it is not enough just one lens, due the fact that the focal length is fixed. In our experiments we needed two lenses to achieve the required waist. At this section we basically have used this formalism only to change the beam waist, however the scope of it covers a wide range of usages, as was said we only need the matrix of a given optical system, that can be anything, not only lenses. Maybe the most notable application of this formalism is the calculus of a complex beam parameter for a stable optical resonator or optical cavity.

4.4 Tilted Lens Method

The experimental results will show features involving topological charge, which are carried by Laguerre – Gaussian beams. However it is impossible to determine the index l via intensity measurements, even for our rather simple space of order 1 modes, due to the fact that the information is encoded in phase, not in amplitude, in contrast to the Hermite-Gaussian modes. Many techniques such as interferometry or far field diffraction were develop to measure accurately the topological charge. The tilted lens [12] is a rather simple but powerful one. The method consists of putting on a spherical lens at a certain distance of the beam waist, and give it a tilt, changing the radial symmetry. It transforms the Laguerre mode to a Hermite one, and the magnitude of the topological charge is shown in the number of nodal lines of the

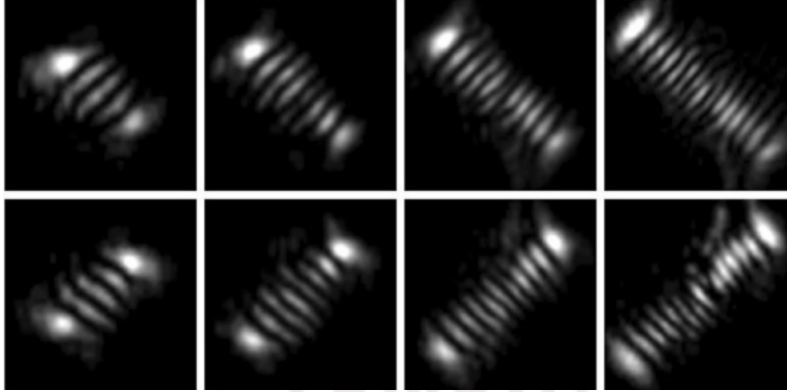


Figure 4.4: These are some results reported by P. Vaity et al. [12] On the top row converted beams carried a topological charge $l = -4, -7, -10, -14$, while in the bottom row $l = +4, +7, +10, +14$. I decided not to show results measured in our experiment because they form part of later discussion.

Hermite mode, while the sign in the inclination, as it was shown with great success by P. Vaity et al., with beams that carry topological charge up to $|l|=14$

Even when this procedure is very useful, much research is still going on towards a complete protocol to identify an arbitrary mode in the OAM sphere, in a similar fashion to the usual tomography performed in the polarization domain via the Stokes parameters.

4.5 Pound Drever Hall Method

Optical cavities for the vast majority of experiments need to work at the resonant length, which is something extremely hard to achieve due to the fact that we would require an accuracy in the order of nanometers. Also, any thermal effect over the air inside the cavity will change the optical path length followed by the beam. So, in practice we require electronic devices that can go beyond the human precision, and help us to maintain the cavity fixed at a given length. The method I am describing is called after their creators [13], and was used in our experiment more than once. First of all, we need the cavity to produce a “remaining”, meaning some sort of light that comes from the cavity and that bring us information about the interference going on inside, aside from the main output signal. It will depend on the

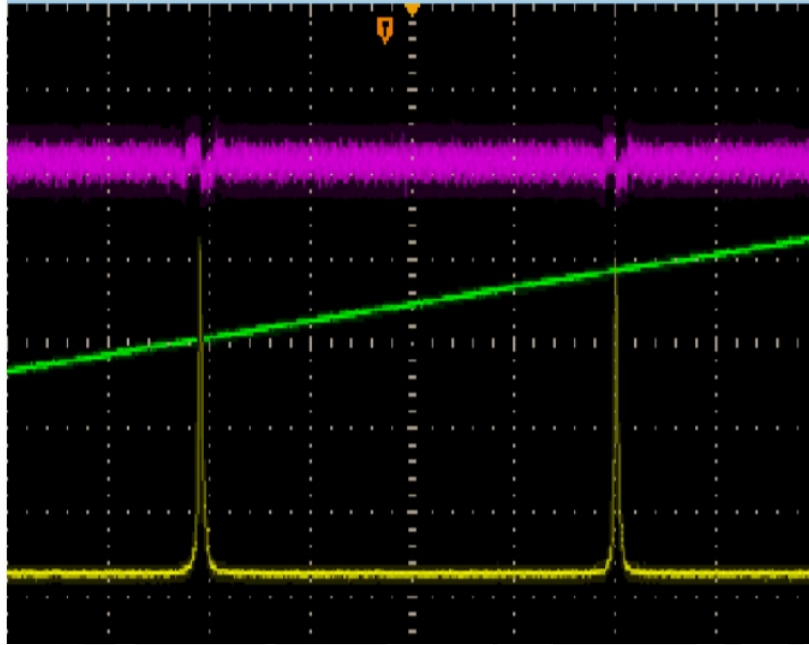


Figure 4.5: here we can see 3 signals, the green one is the triangle signal that is applied to the PZT to scan the resonance lengths of the cavity. The yellow signal is the output of the cavity, that shows peaks whenever the resonance length is passed through. Finally the purple one is referred to the error signal, take notice that when the size of the cavity is approaching the resonance length the error signal is positive, while if we already passed the resonance length it's negative.

specific configuration of our cavity. Also we need to mention piezoelectric (PZT) devices. They change their length depending on the voltage applied. Here we are going to mount a mirror on a PZT that will be fed with a triangle signal, so in that way we are going to be passing through the resonant length many times, and if we connect the main signal to a oscilloscope we will see peaks of intensity.

Now, the way to go is take our “remaining signal”, and pass it through a derivation circuit [13] we get the so-called “error signal”, it is important that the signal that helps us to stabilize the cavity must be the derivative of the “remaining signal” because it can tell us if the PZT is pushing too much, or not the mirror, only using the intensity signal would be useless given its symmetry respect to the peak.

Fortunately enough, the electronics is fast enough to use the “error signal”

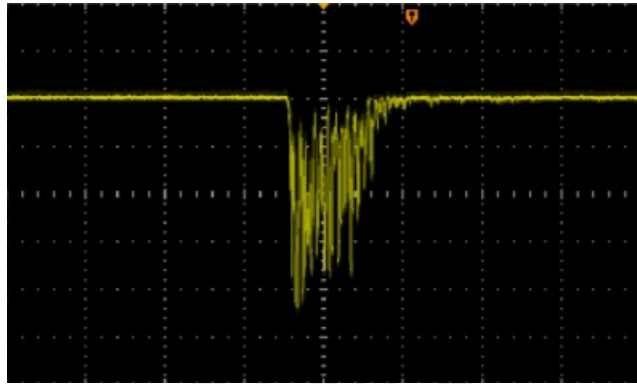
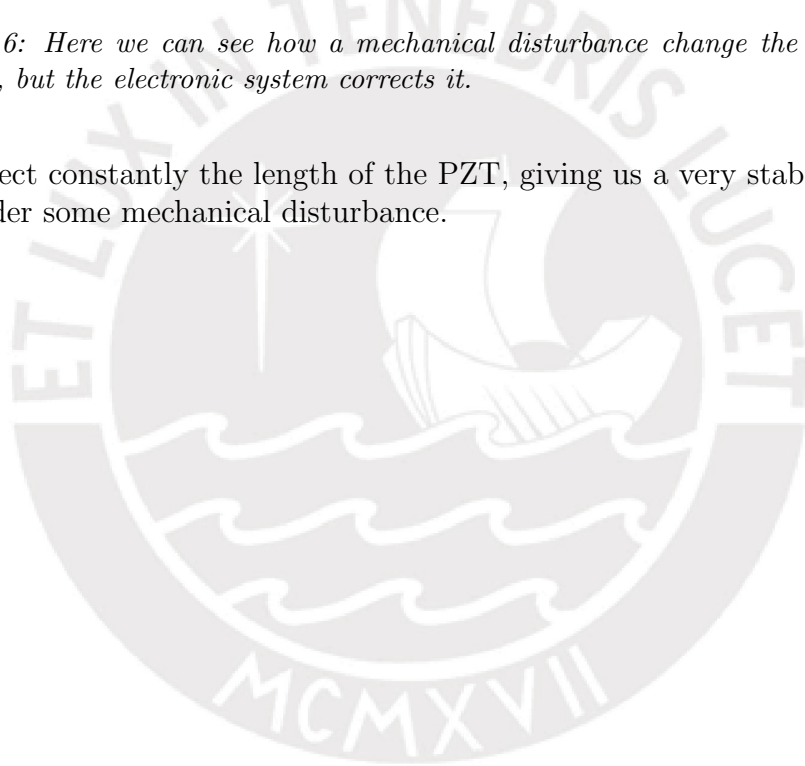


Figure 4.6: Here we can see how a mechanical disturbance change the intensity spectrum, but the electronic system corrects it.

and correct constantly the length of the PZT, giving us a very stable cavity even under some mechanical disturbance.



Chapter 5

Quantum Correlations of Light

We have arrived at a very important and interesting point not exclusively in optics, but in the whole physics, and not only for its intriguing implications but also the applications that are subject of investigation nowadays.

The following discussion will be divided in two parts, the first half will present the standard notion of “Quantum Correlation” and tests, while the second one refers to the experimental methods to achieve such correlations.

5.1 Entanglement

This concept was introduced very long time ago, when the basis of quantum mechanics were still in debate, referred by many as the feature that separates quantum mechanics from the classical one. Nowadays, using the mathematical formalism for quantum mechanics we can formulate a clear definition of entanglement as the impossibility of two systems to be described independently of each other or be written as a tensor product.

$$|\psi_{1,2}\rangle \neq |\psi_1\rangle \otimes |\psi_2\rangle \quad (5.1)$$

It has deep implications in many philosophical and practical considerations, because besides the math that is implied to calculate observables, the result of any measurement done in any constituent of the system will be correlated with its counterpart.

This could lead us to an even bigger trouble if we consider both systems arbitrarily far from each other, far enough to not allow any kind of interaction

after the measurement in one constituent, apparently violating the principle of relativity (no information can travel faster than light).

This fact was topic of many interesting debates in the history of quantum mechanics, that reached its peak when Einstein, Podolsky and Rosen tried to show that quantum mechanics was “incomplete”. It means that the apparent randomness shown by quantum mechanics should be a consequence of variables that were not considered (“hidden variables”). These variables defined the initial conditions of the experiment, and as a consequence the perfect correlation would be natural to be found.

After the publication done by Einstein et al. In 1935 [14], the strongest reply to their claim was the theorem enunciated by J.S.Bell in 1964 [15], where he stated that “No physical theory of local hidden variables can ever reproduce all the predictions on quantum mechanics”. It was based on a calculus analogous to the spin correlation (it could be applied to any two-level system).

The considerations taken were first exist a probability distribution of the hidden variables that determine the outcome of any observable.

$$\int \rho(\lambda) d\lambda = 1 \quad (5.2)$$

The second one is to assume that any measurement is independent from each other:

$$\int P(A(\lambda, a)|B(\lambda, b))\rho(\lambda) d\lambda = \int P(A(\lambda, a))\rho(\lambda) d\lambda \times \int P(B(\lambda, b))\rho(\lambda) d\lambda \quad (5.3)$$

Here A and B are the outcomes of the measurement, while the “a” and “b” the possible configurations of the detectors A and B and the hidden variable is denoted by λ . Now if we consider dichotomic measurements where the outcomes will only be ± 1 , which are analogous to projective measurements in quantum mechanics for two-level systems, it is possible to construct Bell type correlations as:

$$E(a, b) = \int \langle A(\lambda, a) \rangle \langle B(\lambda, b) \rangle \rho(\lambda) d\lambda \quad (5.4)$$

As both averages are less than one, and taking into account equations 5.2 and 5.3, it is possible to write the so called CHSH (Clauser-Horn-Shimony-Holt) [16] inequality:

$$|E(a, b) - E(a, b') + E(a', b') + E(a', b)| \leq 2 \quad (5.5)$$

This expression gives us a boundary that any local and realistic theory should respect. If we compare this with the usual way to take correlations in quantum mechanics:

$$Q(a, b) = \langle (\vec{\sigma} \cdot \vec{a})_1 (\vec{\sigma} \cdot \vec{b})_2 \rangle = \vec{a} \cdot \vec{b} \quad (5.6)$$

Where $\vec{\sigma}$ is the vector made by the Pauli matrices, if we insert 5.6 in equation 5.5 as the new way to take correlations we can realize that choosing some vectors we can break the inequality. In fact, it can be shown that:

$$|Q(a, b) - Q(a, b') + Q(a', b') + Q(a', b)| \leq 2\sqrt{2} \quad (5.7)$$

which is known as the Tsirelson's bound. It is important to see that as quantum mechanics is able to break 5.5 we can claim that it cannot be explained by a model of local hidden variables, and in fact nature shows its quantum behavior in the sense that attains stronger correlations than classical physics. Such feature nowadays has been explored in many applications, mainly in the field of communications and information processing. Our experiment is not an exception, but this is performed not in the way of a correlation test as Bell inequalities, but it uses the stronger correlations of quantum mechanics to reduce the noise of signals.

5.2 Parametric Down Conversion

Nowadays technology has evolved greatly in the regard of non - linear optics, up to the point that the most truthful source of highly correlated photons are crystals constructed with second order susceptibilities $\chi^{(2)}$ that induce processes where the frequency of the incoming light will not be conserved.

In our experiment we used a KTP (Potassium titanyl phosphate) crystal, that has the property of converting the incoming pump photon of frequency corresponding to 532 nm. to a couple of photons of less energy but that must satisfy the energy conservation. For historical considerations, the photons generated are called "signal" and "idler".

$$\omega_p = \omega_s + \omega_i \quad (5.8)$$

Also the generated photons should conserve the momentum. As this condition has a vectorial nature, there exist many geometrical configurations for the new photons to propagate. However, the particularity of the KTP crystal is to make them co-linear with an almost negligible walk-off angle.

$$\vec{k}_p = \vec{k}_s + \vec{k}_i \quad (5.9)$$

Both 5.8 and 5.9 constitute the so called “phase matching condition”. The process is called downconversion because the frequencies of the output photons are lower than the one of the pump.

In our case, the pump photon of 532 nm produces a couple of photons of 1024 nm. There are two types of down-conversion processes differentiated by the polarization of the generated photons. When “signal” and “idler” have the same polarization, they are called of type-I, while when they are orthogonal, they have the denomination of type – II. Our experiment dealt with the last kind.



Chapter 6

Optical Parametric Oscillator

An optical parametric oscillator is just an optical cavity equipped with a crystal that has non-linear interactions with the electric field, giving rise to a wide range of new complex and interesting features due to the new fields that will be generated inside, usually through parametric-down conversion and their interactions. In this Section, I will discuss briefly general non-linear phenomena, and the proper parametric oscillator equations that govern the dynamics of the fields, such as the conditions for their stability.

6.1 Non-linear Susceptibility

As any electromagnetic textbook points out, there exist a relation between the polarization density and the electric field, which is given by:

$$\vec{P} = \chi \vec{E} \quad (6.1)$$

This relation initially operates over the time domain, and hold for any isotropic material. However, our aim is to see the effects of an-isotropic materials on the polarization. In this case, the susceptibility is described by a tensor, while it will be more useful to express the generalization of the above equation in the frequency domain:

$$P_i(\omega) = \chi_{i,j}(\omega)E_j(\omega) + \chi^{(2)}_{i,j,k}(\omega, \omega', \omega'')E_j(\omega')E_k(\omega'') + \dots \quad (6.2)$$

We stop the expansion at the second term of the susceptibility , because in our case higher-order contributions can be neglected . All contributions

have their own frequencies, e.g., ω' and ω'' , which are characteristic of the materials.

It is important not to lose our physical intuition, and ask ourselves what should happen if the incident field is $-\vec{E}$ instead of \vec{E} . As it is an isotropic material, we would expect to get $-\vec{P}$ instead of \vec{P} , which means there could not be any contribution of second order of the susceptibility, because as it is shown in 6.2, they carry quadratic terms of the electric field. In general, any isotropic field cannot have contributions of even order of the susceptibility. Now let us try to see what kind of processes arise from the existence of the second order. As was said before, there must be two frequencies allowed by the material, so let us start assuming the electric field is a superposition of the following form:

$$\vec{E} = \vec{E}_1 e^{i(\vec{k}_1 \cdot \vec{r} - \omega_1 t)} + \vec{E}_2 e^{i(\vec{k}_2 \cdot \vec{r} - \omega_2 t)} + c.c. \quad (6.3)$$

So the cross terms affected by the second order susceptibility tensor will be :

$$\begin{aligned} \vec{E} \cdot \vec{E} &= \vec{E}_1 \cdot \vec{E}_1 e^{2i(\vec{k}_1 \cdot \vec{r} - \omega_1 t)} + \vec{E}_2 \cdot \vec{E}_2 e^{2i(\vec{k}_2 \cdot \vec{r} - \omega_2 t)} + c.c. \\ &\vec{E}_1 \cdot \vec{E}_1^* + \vec{E}_2 \cdot \vec{E}_2^* \\ &\vec{E}_1 \cdot \vec{E}_2 e^{i[(\vec{k}_1 + \vec{k}_2) \cdot \vec{r} - (\omega_1 + \omega_2)t]} + c.c. \\ &\vec{E}_1 \cdot \vec{E}_2^* e^{i[(\vec{k}_1 - \vec{k}_2) \cdot \vec{r} - (\omega_1 - \omega_2)t]} + c.c. \end{aligned} \quad (6.4)$$

The first two terms correspond to the so called “second harmonic generation”. This name is due to fact that the contributions show the double of the original frequencies.

The third and fourth terms are called “optical rectification”.

The penultimate term as can be inferred for the resulting frequency, is called “frequency sum”, and finally the last one is of especial interest for us, and it is called “frequency subtraction” [17].

The importance of each term will depend directly on the structure of the material, that is reflected in the form of the second order of the susceptibility tensor.

6.2 Subtraction of Frequencies

This process involves the mixture of three waves, where the form of the susceptibility tensor plays a major role. Of course, $\chi^{(2)}(\omega_1, \omega_2, \omega_3 = \omega_1 - \omega_2) \neq 0$, the non linear polarization induced will have the form [17] :

$$P_i(\omega_3 = \omega_1 - \omega_2) = \chi^{(2)}_{i,j,k} E_j^{(1)} E_k^{(2)*} e^{i[(\vec{k}_1 - \vec{k}_2) \cdot \vec{r} - (\omega_1 - \omega_2)t]} \quad (6.5)$$

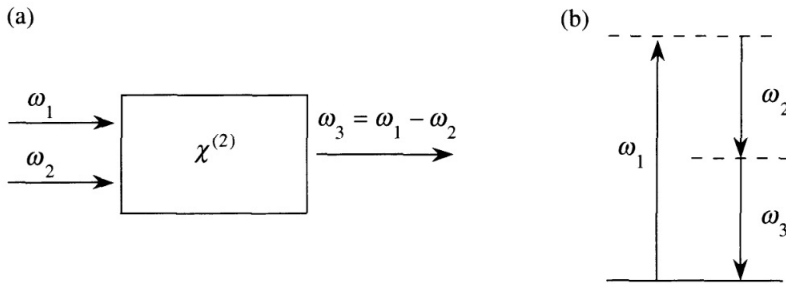


Figure 6.1: Part (a) shows the incoming beams in the process and the constrain for the generated frequency, part (b) shows the energy diagram of the process. Images taken from “Nonlinear Optics” by Robert W. Boyd

A very enlightening commentary is made by Boyd in his textbook about the nature of this process. He points out that the energy conservation of the process imposes the condition that each photon created at the frequency $\omega_3 = \omega_1 - \omega_2$ must be a consequence of the destruction of a higher frequency photon (according to the Figure 6.1 ω_1) and a creation of a lower frequency photon.

In this sense, the process is sometimes called “optical parametric amplification” due to the fact that the lower frequency signal will be amplified. In this way we can approach a basic mental picture of what is an Optical Parametric Oscillator (OPO) : it will be a subtraction frequency process amplified by the fact that the non-linear element will be inside an optical resonator. This will help to build more intense fields (signal e idler) at the price of an optical source feed (pump field).

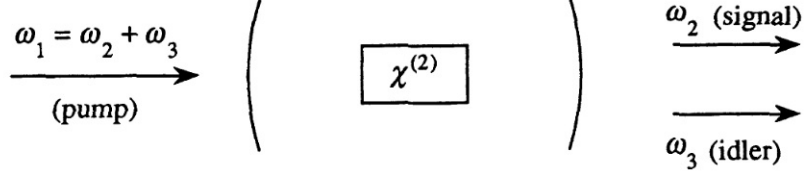


Figure 6.2: Basic dynamics of the Optical Parametric Oscillator, here we can see the only one pump field is required (source to destroy the required photon), this process can take the vacuum as the field to get amplified due to the fact that it's not mandatory to have 2 incoming fields to get the oscillation going. Images taken from "Nonlinear Optics" by Robert W. Boyd

6.3 Dynamic Equations

So finally we are going to describe the core of our experiment. We are going to describe the interaction of three fields inside the optical resonator (pump, signal and idler that will label their fields with the initial letter of their names), equipped with a non-linear crystal (KTP). The dynamic equations deduced by Debuisschert et al. [18] are:

$$\begin{aligned}
 \frac{\partial A_p}{\partial z} &= -\alpha_p A_p + i \frac{\chi \omega_p}{2\eta_p c} A_s A_i \\
 \frac{\partial A_s}{\partial z} &= -\alpha_s A_s + i \frac{\chi \omega_s}{2\eta_s c} A_p A_i^* \\
 \frac{\partial A_i}{\partial z} &= -\alpha_i A_i + i \frac{\chi \omega_i}{2\eta_i c} A_p A_s^*
 \end{aligned} \tag{6.6}$$

Here we are assuming the perfect phase matching condition $\Delta k = \vec{k}_p - \vec{k}_s - \vec{k}_i = 0$, with α_j the loss coefficient due to the crystal, η_j the refraction index and χ is the coupling coefficient, $j = p, s, i$ any time that the index j appears, it means that the equations hold for the three fields.

Now we need to make some approximations to get equations that describe the dynamics in the time domain. Let us start assuming that the change over time will be related to the change in space inside the crystal as :

$$\begin{aligned}
A'_p &\approx A_p + l \frac{\partial A_p}{\partial z} \\
A'_s &\approx A_s + l \frac{\partial A_s}{\partial z} \\
A'_i &\approx A_i + l \frac{\partial A_i}{\partial z}
\end{aligned} \tag{6.7}$$

So combining equations 6.6 and 6.7 we can get rid of the spatial dependence. Now analyzing the field in the whole cavity, its change will be given by:

$$\begin{aligned}
A_p(t + \tau) &\approx A_p(t) \left[1 - 2\alpha_p l - \left(\frac{T_{1,p} + T_{2,p}}{2} \right) + i\Delta_p \tau \right] \\
&\quad + i \frac{\chi \omega_p l}{\eta_p c} A_s A_i + \sqrt{T_{1,p}} A_{p,in}
\end{aligned} \tag{6.8}$$

The T refers to the transmission coefficient of the mirror, τ the time for a round trip of the light and A_p , in the initial amplitude of the field entering the cavity before the reflections. Analogously for the other fields, so in fact if we approximate the total time derivative as:

$$\frac{dA_j}{dt} \approx \frac{A_j(t + \tau) - A_j(t)}{\tau} \tag{6.9}$$

We can write the OPO equations in terms of time as:

$$\begin{aligned}
\frac{dA_p}{dt} &\approx (-\gamma_p + i\Delta_p) A_p + i \frac{\chi \omega_p l}{2\eta_p c \tau} A_s A_i + \frac{\sqrt{T_{1,p}}}{\tau} A_{p,in} \\
\frac{dA_s}{dt} &\approx (-\gamma_s + i\Delta_s) A_s + i \frac{\chi \omega_s l}{2\eta_s c \tau} A_p A_i^* + \frac{\sqrt{T_{1,s}}}{\tau} A_{s,in} \\
\frac{dA_i}{dt} &\approx (-\gamma_i + i\Delta_i) A_i + i \frac{\chi \omega_i l}{2\eta_i c \tau} A_p A_s^* + \frac{\sqrt{T_{1,i}}}{\tau} A_{i,in}
\end{aligned} \tag{6.10}$$

With $\gamma_j = \frac{T_{1,j} + T_{2,j} + 2\alpha_j l}{\tau}$ and Δ_j the detuning of the cavity for each field. Now a very comfortable re-scaling of the equations will prove to be useful for numerical simulation later on. So the new equations are:

$$\begin{aligned}
\frac{da_p}{dt} &= (-\gamma_p + i\Delta_p)a_p - ga_s a_i + \eta_p a_{p,in} \\
\frac{da_s}{dt} &= (-\gamma_s + i\Delta_s)a_s - ga_p a_i^* + \eta_s a_{s,in} \\
\frac{da_i}{dt} &= (-\gamma_i + i\Delta_i)a_i - ga_p a_s^* + \eta_i a_{i,in}
\end{aligned} \tag{6.11}$$

With $a_{p/s} = \frac{\sqrt{n_{p/s}}}{\omega_{p/s}} A_{p/s}$, $a_i = -i \frac{\sqrt{n_i}}{\omega_i} A_i$, $a_{j,in} = -i \frac{\sqrt{n_j}}{\omega_j} A_{j,in}$, $\eta_j = \frac{\sqrt{T_j}}{\tau}$ and $g = \frac{l\chi}{c\tau} \frac{\sqrt{\omega_i \omega_s \omega_p}}{n_i n_s n_p}$

6.4 Stationary Solutions

We are interested in the stationary solutions, i.e. the solution that does not depend on time. In order to get an analytical solution, we will take some considerations:

$$\begin{aligned}
i) a_{s,in} &= a_{i,in} = 0 \\
ii) \gamma_s &= \gamma_i = \gamma \\
iii) \Delta_p &= \Delta_s = \Delta_i = 0
\end{aligned} \tag{6.12}$$

The first condition is very natural, as was already stated, we have enough with only applying the greater frequency field (pump), the nonlinear process will amplify the fields inside the cavity, but in principle it is possible to take them into account.

The second condition tells us that the losses are the same for the signal and idler fields, which is to be expected if we consider both with the same frequency. The last condition is known as ‘‘triple resonant’’ condition, and assumes that the cavity is perfectly resonant for the three fields, which can be achieved in practice if the wavelengths of the fields are integer multiples of one another.

So the new equations that rule our process are:

$$\begin{aligned}
0 &= -\gamma_p a_p - ga_s a_i + \eta_p a_{p,in} \\
0 &= -\gamma a_s + ga_p a_i^* \\
0 &= -\gamma a_i + ga_p a_s^*
\end{aligned} \tag{6.13}$$

Let us write the fields in the polar form: $a_j = r_j e^{i\theta_j}$, without losing generality we can set the phase $\theta_{p,in} = 0$, because the important quantity is the phase difference, so we take the input field as the reference. Taking these considerations into account and inserting them into 6.13 we arrive to a relation between the phases:

$$\begin{aligned}\theta_p &= 0 \\ \theta_s + \theta_i &= 0\end{aligned}\tag{6.14}$$

It is interesting to see that the phase difference of signal and idler is not fixed. Now from 6.13 and 6.14 we can deduce:

$$r_s^2 = r_i^2\tag{6.15}$$

Equation 6.15 tells us that the intensities will always be the same for signal and idler (this situation should change if we do not consider i) in 6.12), but also we see that there are two solutions:

The trivial solution $r_s = r_i = 0$ that leads us to:

$$\begin{aligned}I_s &= I_i = 0 \\ I_p &= \left(\frac{\eta_p a_{p,in}}{\gamma}\right)^2\end{aligned}\tag{6.16}$$

This solution is almost like if there is no crystal, i.e., no amplification. The second solution, that we are going to call ‘‘OPO solution’’, is given when $r_s = r_i = r$, this leads us to:

$$\begin{aligned}I_p &= \left(\frac{\gamma}{g}\right)^2 \\ I_{s/i} &= I = \frac{1}{g} \left(\eta_p a_{p,in} - \frac{\gamma \gamma_p}{g}\right)\end{aligned}\tag{6.17}$$

The last expression constitutes a very interesting feature of the OPO system. As we can see, the intensity of the pump field is constant. It stops to depend from the input field, which tells us that it does not matter if we inject a high intensity to the cavity. The intensity of the field at the output

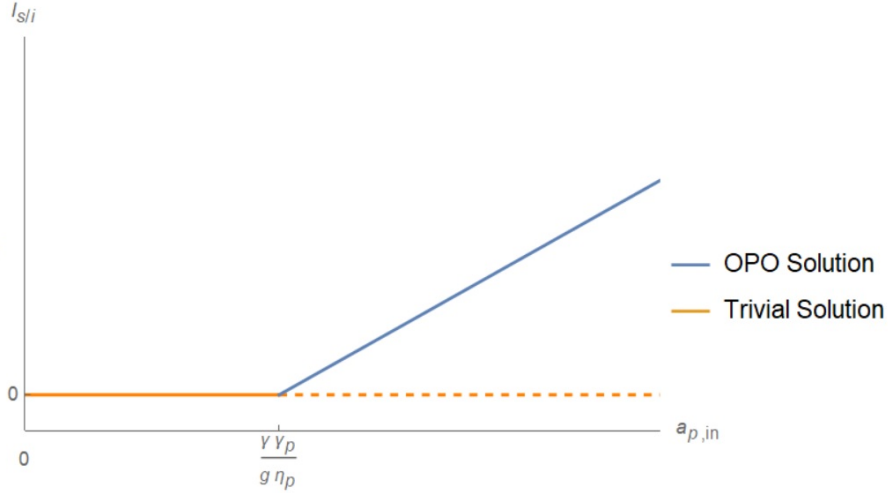


Figure 6.3: This graphic shows the OPO dynamics, where after a threshold value appears the OPO solution that brings to life the signal and idler fields.

will not grow anymore; of course, the energy should go somewhere, and the answer is in the second equation of 6.17.

As we know that the intensity should be always be positive, the second equation of 6.17 gives us a condition for the “OPO solution” to appear:

$$a_{p,in} \geq \frac{\gamma\gamma_p}{g\eta_p} \quad (6.18)$$

This is called the threshold of oscillation, since at this point the amplification appears on the signal and idler fields, and the input intensity is totally employed in the amplification process.

It is important to recall that below the threshold only the trivial solution is possible. Once we pass this mark, it appears the OPO solution. However, the trivial solution still is possible, in fact both solutions coexist in this regime, the solution chosen by the system to operate in, depends on the stability of each one.

6.5 Stability

Now we are going to make a stability analysis of the OPO dynamics described by 6.11. We suppose that fields slightly deviate from their steady values :

$$\begin{aligned}
a_j &= a_{j,0} + \delta a_j \\
a'_j &= \delta a'_j
\end{aligned}
\tag{6.19}$$

Here $a_{j,0}$ represents the field in the equilibrium state, so equations in 6.13 only hold for these fields in equilibrium. Inserting 6.19 in 6.11, and omitting second order terms in the variation, we get a new set of equations:

$$\begin{aligned}
\delta a'_p &= -\gamma_p \delta a_p - g a_{s,0} \delta a_i - g a_{i,0} \delta a_s \\
\delta a'_s &= -\gamma \delta a_s - g a_{p,0} \delta a^*_i - g a^*_{i,0} \delta a_p \\
\delta a'_i &= -\gamma \delta a_p - g a_{p,0} \delta a^*_s - g a^*_{s,0} \delta a_p
\end{aligned}
\tag{6.20}$$

Equations in 6.20 are a coupled linear system, the solutions for $\delta a_j(t)$ should be proportional to exponentials of the form $e^{\lambda t}$, and the stability condition will be given by the real part of lambda. If $Re(\lambda) \leq 0$ the system will oscillate around a stationary value, so that $\delta a'_j = \lambda \delta a_j$. Now let us try to decouple the system through:

$$\begin{aligned}
a_j &= X_j + iY_j \\
\delta a_j &= \delta X_j + i\delta Y_j
\end{aligned}
\tag{6.21}$$

Using the ansatz described and 6.21 we get two systems of equations for X and Y, but do not forget that we want to determine the stability above threshold of oscillation. This implies, according to 6.17 for the ‘‘OPO solution’’, that $a_{p,0} = \frac{\gamma}{g}$ and $a_{s,0} = a_{i,0} = \sqrt{\frac{\eta_p a_{p,in}}{g} - \frac{\gamma \gamma_p}{g^2}}$. The phase relations described in 6.14 still hold. We are allowed to pick a value $\theta_{s,0} = \theta_{i,0} = 0$ due to the indetermination of the phase difference. Taking these considerations into account the decoupling will take some specific values:

$$\begin{aligned}
X_{p,0} &= \frac{\gamma}{g} \\
Y_{p,0} &= 0 \\
X_{s,0} &= X_{i,0} = r \\
Y_{s,0} - Y_{i,0} &= 0
\end{aligned}
\tag{6.22}$$

Using 6.21 and 6.22 we can rewrite 6.20 for the real part X in matrix form:

$$\begin{pmatrix} \delta X'_p \\ \delta X'_s \\ \delta X'_i \end{pmatrix} = \begin{pmatrix} \gamma_p & -gr & -gr \\ gr & -\gamma & \gamma \\ gr & \gamma & -\gamma \end{pmatrix} \cdot \begin{pmatrix} \delta X_p \\ \delta X_s \\ \delta X_i \end{pmatrix} \quad (6.23)$$

And for the imaginary part

$$\begin{pmatrix} \delta Y'_p \\ \delta Y'_s \\ \delta Y'_i \end{pmatrix} = \begin{pmatrix} \gamma_p & -gr & -gr \\ gr & -\gamma & -\gamma \\ gr & -\gamma & -\gamma \end{pmatrix} \cdot \begin{pmatrix} \delta Y_p \\ \delta Y_s \\ \delta Y_i \end{pmatrix} \quad (6.24)$$

Let us call the matrix of coefficients for the real part M_x while for the imaginary part M_y . Now our problem has been reduced to find the eigenvalues of these two coefficient matrices, which is very easy to perform obtaining for M_x .

$$\begin{aligned} \lambda_{x,1} &= -2\gamma \\ \lambda_{x,2} &= -\frac{1}{2}(\gamma_p + \sqrt{\gamma_p^2 - 8g^2r^2}) \\ \lambda_{x,3} &= -\frac{1}{2}(\gamma_p - \sqrt{\gamma_p^2 - 8g^2r^2}) \end{aligned} \quad (6.25)$$

It is obvious that $Re(\lambda_{x,1}) \leq 0$, while for the remaining two if the square root gives us an imaginary value clearly both $Re(\lambda_{x,2/3}) \leq 0$. In case that the square root remains real the highest value that can be reached will be γ_p so $Re(\lambda_{x,2}) = -\gamma_p$ and $Re(\lambda_{x,3}) = 0$. For M_y the eigenvalues are:

$$\begin{aligned} \lambda_{y,1} &= 0 \\ \lambda_{y,2} &= -\frac{1}{2}[(2\gamma + \gamma_p) + \sqrt{(\gamma_p - 2\gamma)^2 - 8g^2r^2}] \\ \lambda_{y,3} &= -\frac{1}{2}[(2\gamma + \gamma_p) - \sqrt{(\gamma_p - 2\gamma)^2 - 8g^2r^2}] \end{aligned} \quad (6.26)$$

Following the same reasoning described above, we can conclude that both coefficient matrices fulfill the condition $Re(\lambda_{OPOsol}) \leq 0$, so in fact the ‘‘OPO solution’’ is stable once we pass the threshold of oscillation.

We can check also the stability of the trivial solution, for which we just need to rewrite equation 6.20 considering $a_{s,0} = a_{i,0} = 0$ and $a_{p,0} = \frac{\eta_p a_{p,in}}{\gamma_p}$

$$\begin{aligned}
\delta a'_p &= -\gamma_p \delta a_p \\
\delta a'_s &= -\gamma \delta a_s + g a_{p,0} \delta a^*_i \\
\delta a'_i &= -\gamma \delta a_i + g a_{p,0} \delta a^*_s
\end{aligned} \tag{6.27}$$

Now we do not need to focus on the equation related to the pump field because it is an independent one. We can perform again the decoupling in terms of X and Y, as was already done, and our coefficient matrices will be now 2×2 .

$$\begin{pmatrix} \delta X'_s \\ \delta X'_i \end{pmatrix} = \begin{pmatrix} -\gamma & g a_{p,0} \\ g a_{p,0} & -\gamma \end{pmatrix} \cdot \begin{pmatrix} \delta X_s \\ \delta X_i \end{pmatrix} \tag{6.28}$$

$$\begin{pmatrix} \delta Y'_s \\ \delta Y'_i \end{pmatrix} = \begin{pmatrix} -\gamma & -g a_{p,0} \\ -g a_{p,0} & -\gamma \end{pmatrix} \cdot \begin{pmatrix} \delta Y_s \\ \delta Y_i \end{pmatrix} \tag{6.29}$$

Both matrices have the same eigenvalues

$$\lambda = -\gamma \pm g a_{p,0} \tag{6.30}$$

The condition $Re(\lambda) \leq 0$ will be only fulfilled for both eigenvalues if $a_{p,0} \leq \frac{\gamma}{g}$, which is the threshold of oscillation. This means that the trivial solution is stable below the threshold, and unstable above it.

The discussion was intended to show that the OPO is a dynamical system that works as described by the trivial solution until we pass the threshold of oscillation. There the system behaves according to the stable solution, which corresponds to the ‘‘OPO solution’’.

6.6 Numerical Simulation

Up to this point, we have made various approximations to achieve an analytical solution, but nowadays there are many softwares like ‘‘Wolfram Mathematica’’ or ‘‘Matlab’’ that make numeric analysis much easier and are very powerful tools to use when we are not able to get an analytical solution.

Now we are going to briefly discuss the implications of ignoring 6.12. This treatment is not completely rigorous because I am setting the parameters to real values, without taking care of units or normalizations, even though it will help us to get a feeling of the qualitative behavior of the system.

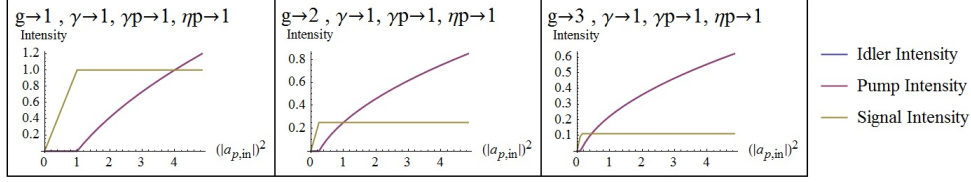


Figure 6.4: Numerical simulation of the dynamic of the OPO, the idler and signal intensities are overlap because they have the same intensity in the process. This legend holds for all the other simulations.

First let us see the changes when the coupling constant gets higher. As it is shown in Figure 6.4 the threshold of oscillation gets lower and lower, which is intuitively right. We expect that for a very small coupling constant we would need to apply an enormous energy to achieve an oscillation. This behavior is expected for any coupled dynamical system.

In this way we can start to vary the parameters, changing the losses of the signal and idler fields. We can see in Figure 6.5 that the threshold of oscillations gets higher and the stationary intensity of the pump field is also higher.

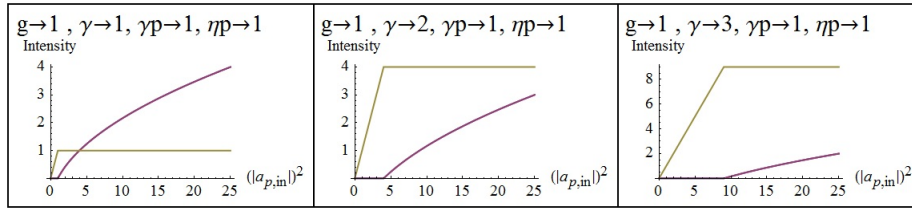


Figure 6.5

Now, if we change the loss coefficient of the pump field, we obtain the results shown in Figure 6.6. As a consequence, the threshold is higher, because the energy injected to the cavity is getting scattered.

Now changing η_p , Figure 6.7 shows us that the threshold gets smaller, which is a very counterintuitive feature, because remember that $\eta_p = \frac{\sqrt{T_p}}{\tau}$. The round trip time is a fixed value because it is related to the cavity length, so the way to get a higher η_p is to use mirrors with higher transmission coefficient. In fact, it should lead to a lower value for the intracavity energy. However, the graphics in Figure 6.7 represent the relation written in equation

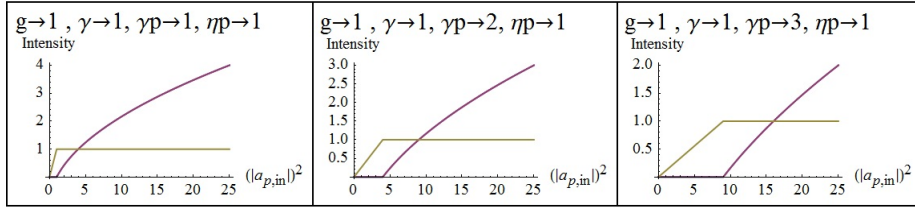


Figure 6.6

6.18.

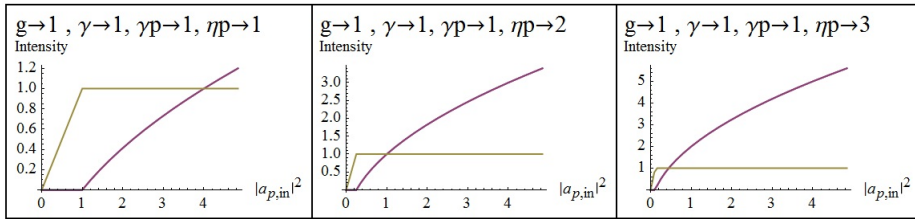


Figure 6.7

Finally I tried to change a parameter that was kind of intriguing for me at the beginning of this work, which is the detuning parameter, in fact the experimental work always focus in the alignment of the cavity which of course means, to work in the resonant regime, but of course this process requires dexterity and experience. Figure 6.8 shows some interesting features in this regard.

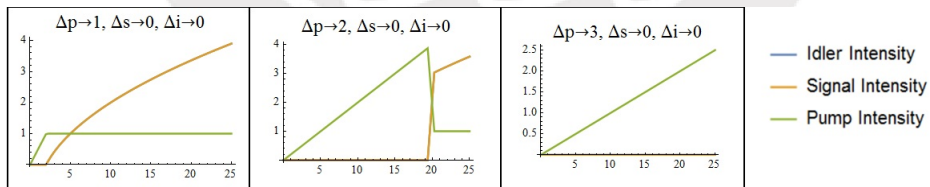


Figure 6.8

The first graphic shows the typical dynamics, while the third one shows that the threshold is much higher than in graphic 1. It tells us that the threshold is very sensitive to detuning of the pump field. The second graphic is in some sense weird, as it differs from the previous ones because there

seems to exist two critical points. Because the generated signal and the pump exhibit two changes in behavior, this is a very interesting feature, and it is a consequence of the detuning. There seems to exist a bi-stability regime for some values of the detuning, and the initial conditions will be the only factor that determines in which way our resonator will oscillate. Of course, this requires a much more throughout treatment, one that lies beyond the scope of the present work.



Chapter 7

Squeezing

Now we are going to review very briefly some aspect about the quantum harmonic oscillator and coherent states. This will lead us to the uncertainty relations, which are the target of the squeezing experiment. Much of this discussion is based on some topics of quantum mechanics that can be found in textbooks [19].

7.1 Coherent States

Here it is convenient to change the classical notation used for the quantization of the electromagnetic field, and write Y instead of P . This will prove to be useful later, so our ladder operator, setting $m\omega = 1$ for simplicity, will be :

$$\begin{aligned}\hat{a}_\mu &= \frac{\hat{X}_\mu + i\hat{Y}_\mu}{\sqrt{2\hbar}} \\ \hat{a}_\mu^\dagger &= \frac{\hat{X}_\mu - i\hat{Y}_\mu}{\sqrt{2\hbar}}\end{aligned}\tag{7.1}$$

The lower index μ labels the mode of the electromagnetic field. Now using the usual way to calculate the standard deviation for an operator:

$$\Delta O = \sqrt{\langle O^2 \rangle - \langle O \rangle^2}\tag{7.2}$$

we can calculate the form of the product of standard deviations for the canonical variables X and Y . Using the Fock basis:

$$(\Delta X \Delta Y)_n = \left(n + \frac{1}{2}\right) \hbar \quad (7.3)$$

So in the Fock space only the vacuum state has the lowest uncertainty value $\frac{\hbar}{2}$. Now let us recall the result for the coherent state. It is important in this work due to the fact that lasers deliver light in an almost coherent state light, We remind that

$$\hat{a}|v\rangle = v|v\rangle \quad (7.4)$$

So the new standard deviations are

$$\Delta X = \Delta Y = \sqrt{\frac{\hbar}{2}} \quad (7.5)$$

It is clear now that any coherent state works in the lowest value of the uncertainty relationship, independently of the specific state.

$$(\Delta X \Delta Y)_v = \frac{\hbar}{2} \quad (7.6)$$

We can represent the uncertainty relationship as an area in the phase space, see Figure 7.1.

7.2 Generalized Quadratures

Now we would like to achieve states that still operate in the lowest uncertainty value, but have different standard deviations for each canonical variable, called “quadratures”. To get this we need to introduce the squeeze operator.

$$U(z) = \exp z\hat{a}^2 - z^*\hat{a}^{\dagger 2} \quad (7.7)$$

It is easy to verify that is a unitary operator. Now we will define the squeezed vacuum state as:

$$U(z)|0\rangle = |0, z\rangle \quad (7.8)$$

The first index on the right hand side will be left as zero because it is designed to change under the displacement operator, which is explained later. For the explicit calculation of the standard deviations, it will be useful to have the next term pre-calculated:

$$U^\dagger(z)\hat{a}U(z) \quad (7.9)$$

This is important because the expected values in the quadratures will involve terms in the form of $\hat{a}^{\dagger 2}, \hat{a}^2, \hat{a}\hat{a}^\dagger$, which can be deduced from 7.9 by taking the complex conjugate and inserting the identity $U^\dagger.U = 1$ in convenient places. Using the Baker – Hausdorff identity and writing the complex number in polar form $z = re^{i\theta}$ equation 7.9 takes the form

$$U^\dagger(z)\hat{a}U(z) = \hat{a} \cosh 2r - \hat{a}^\dagger e^{-i\theta} \sinh 2r \quad (7.10)$$

From this we can follow the same procedure, and calculate the standard deviations for \hat{X} and \hat{Y} described in terms of the ladder operators in 7.1. The expected values are:

$$\langle 0, z | \hat{a} | 0, z \rangle = \langle 0 | U^\dagger(z)\hat{a}U(z) | 0 \rangle \quad (7.11)$$

As a consequence:

$$\langle X \rangle_{0,z} = \langle Y \rangle_{0,z} = 0 \quad (7.12)$$

The lower indexes are only to remember over which state we take the expected value:

$$\begin{aligned} \langle X^2 \rangle_{0,z} &= \frac{\hbar}{2} e^{-2r} \\ \langle Y^2 \rangle_{0,z} &= \frac{\hbar}{2} e^{2r} \end{aligned} \quad (7.13)$$

Finally, the standard deviations are:

$$\begin{aligned} \Delta X &= \sqrt{\frac{\hbar}{2}} e^{-r} \\ \Delta Y &= \sqrt{\frac{\hbar}{2}} e^r \end{aligned} \quad (7.14)$$

With this approach, we could keep the lowest uncertainty value $\Delta X \Delta Y = \frac{\hbar}{2}$ while breaking the symmetry in the standard deviations 7.14.

Now we want to displace this state from the origin, to be able to talk about quadratures of Phase and Module. We can define generalized quadratures as:

$$\begin{aligned}\hat{X}(\theta) &= \hat{X} \cos \theta + \hat{Y} \sin \theta \\ \hat{Y}(\theta) &= \hat{X} \sin \theta + \hat{Y} \cos \theta\end{aligned}\tag{7.15}$$

described in terms of ladder operators

$$\begin{aligned}\hat{X}(\theta) &= \sqrt{\frac{\hbar}{2}}(\hat{a}e^{-i\theta} + \hat{a}^\dagger e^{i\theta}) \\ \hat{Y}(\theta) &= \sqrt{\frac{\hbar}{2}}\frac{(\hat{a}e^{-i\theta} - \hat{a}^\dagger e^{i\theta})}{i}\end{aligned}\tag{7.16}$$

With these new quadratures, we want to achieve $\langle X \rangle \neq 0$ and $\langle Y \rangle \neq 0$ which is possible only if we squeeze a state that is not the vacuum 7.8. This is important because as the uncertainty region will not be centered in the origin, we can talk about a module and phase of the complex number that shifts the region in the phase space. For this purpose, we define the displacement operator:

$$\hat{D}(v) = \exp v\hat{a}^\dagger - v^*\hat{a}\tag{7.17}$$

Again, it is illustrative to write the complex number in polar form $v = re^{i\theta}$, and merging this with 7.16 the displacement operator is:

$$\hat{D}(v) = e^{\frac{-i}{\hbar}R(\theta)\hat{Y}(\theta)}, \text{ with } r = \frac{R(\theta)}{\sqrt{2\hbar}}\tag{7.18}$$

Now it is clear why this is called the displacement operator when we compare it with the Translation operator $\hat{T}(x) = e^{\frac{-i}{\hbar}\hat{P}x}$. In this case, the translation will be given in the direction of $R(\theta)$. Now the displacement operates over the vacuum in the following way:

$$\hat{D}(v)|0\rangle = |v\rangle\tag{7.19}$$

which is the last piece we needed. Now we can define the general squeezed state as

$$\hat{D}(z)\hat{U}(z)|0\rangle = |v, z\rangle\tag{7.20}$$

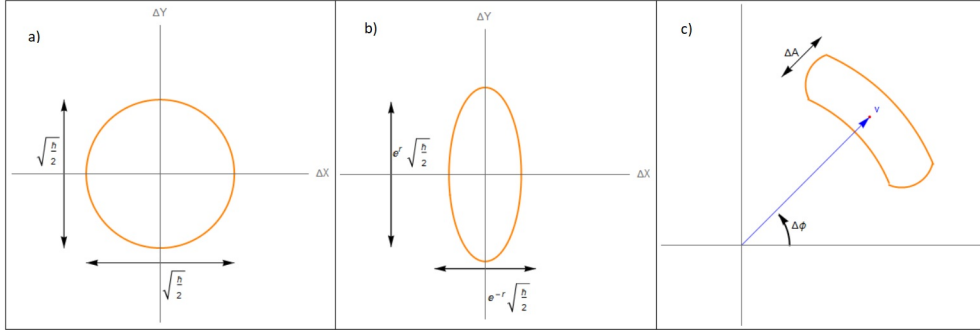


Figure 7.1: The a) image shows the uncertainty region which is a circle due to the symmetry in both standard deviations for the Fock space, b) shows the same uncertainty relation once we apply the squeezing operator to our state and take the expected values on the coherent state space. Finally c) shows the generalized quadrature in the phase space, there is important to see that it's possible to talk about compression in Amplitude and Phase due to the fact that we are outside the origin.

7.3 Experimental Results

My work at the UFF was done in collaboration with Prof. Carlos Eduardo Souza, Prof. Renné Medeiros and the master student Rafael Bellas. They had already performed the squeezing measurements, so the results that I am going to show in this section correspond to a re-run of their previous experiment. Rafael Bellas was the main person who manipulated the experiment due to his experience, He taught me the “know how” of the OPO, something for which I am very grateful.

Now we follow the work done by A. Heidmann et al. [20] They show that if a non-linear crystal (as the KTP) is inserted in a optical resonator, the twin photons generated by the parametric conversion oscillates, as was already stated in previous sections, but the new feature is that the intensities of the signal and idler field are better correlated than the Shot Noise Limit (correlation of two random signals). This kind of correlation is a consequence of the squeezing of the amplitude difference between the signal and idler fields. Of course, if we compress the amplitude, we would obtain larger standard deviations in the phase quadrature, but this work will only show results in amplitudes.

An intuitive way to understand this phenomenon is in terms of the twin

photons generated by the KTP crystal. They are highly correlated. However, they do not go to the last mirror together, they are kept inside the cavity for a characteristic time, determined by the transmission coefficient of the mirrors. In this way, it is build an intense beam. Of course, if we diminish the transitivity of the mirrors, the intensity will be smaller. The threshold gets higher as eq. 6.18 suggests, but as it is easier for the twin photons to go outside together they will be more correlated. Of course, if we only pump the KTP without optical resonator, we would need photo-counters, and the correlations will be more of the kind discussed in the chapter 5, but this is not the point, we want to build up a beam with macroscopic intensity properties. In this sense there is a trade-off between the threshold of oscillation and the squeezing measurement, both aspects need to be taken into account when we design the experiment.

The scheme of the squeezing experiment is seen in Figure 7.2. We used as a pump beam a Nd:YAG laser (Model: Diabolo Innolight Laser) that works in the $TEM_{0,0}$ with a wavelength of 530 nm (green line). This laser has a second output of infrared light at 1064 nm, which is useful in this experiment to calibrate the shot noise limit (later it will play a major role). The pump beam first passes through a Fabry – Perot interferometer, to be cleaned in this locked triangular filter cavity, then passes an optical isolator, which avoids the return of the pump beam to the laser. Without the latter, the reflection could damage the laser. The lenses l1 and l2 are used to mode-matching the pump beam to the OPO cavity. The semi-monolithic OPO consists of a 10 mm long KTP crystal and a spherical mirror with radius of curvature of 5 cm., the input face of the crystal is coated to act as the OPO input coupler (reflectivity 92 % at 532 nm.) while the other face is AR-coated. The concave mirror of the OPO cavity is mounted on a piezoelectric transducer (PZT). The OPO was set in a near concentric configuration with a beam waist of 63 μ m, approximately. The OPO cavity is very unstable, so that the crystal and the mirror are enclosed in a box, and also the crystal has a temperature control (within a few millikelvin). All the cavities in the experiment have electronic equipment to apply the Pound-Drever-Hall method, and keep them stable.

The KTP crystal emits the twin photons with orthogonal polarizations and in a col-linear configuration. We need then a first a mirror that only let the signal and idler beams (1024 nm) pass through, filtering the pump beam. Then, with a PBS (Polarization Beam Splitter) we can separate the twin photons. Using the signal that is gotten by the fast detectors (2 and

3) we can obtain the difference of the intensities with an electronic circuit. Finally, with a spectrum analyzer we can see the noise reduction.

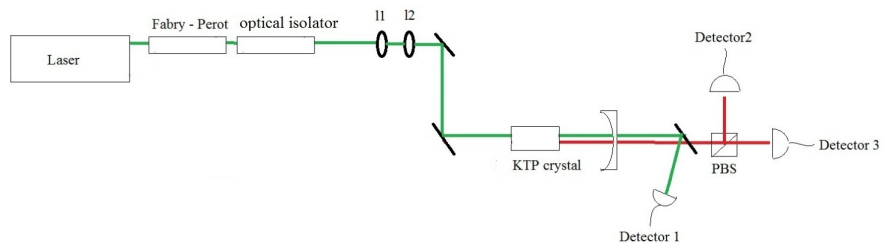


Figure 7.2: Experimental setup of the squeezing measurement

The resulting spectra are shown in Figure 7.3. There we can see that the difference of intensity spectrum is under the shot noise level, showing a noise compression.

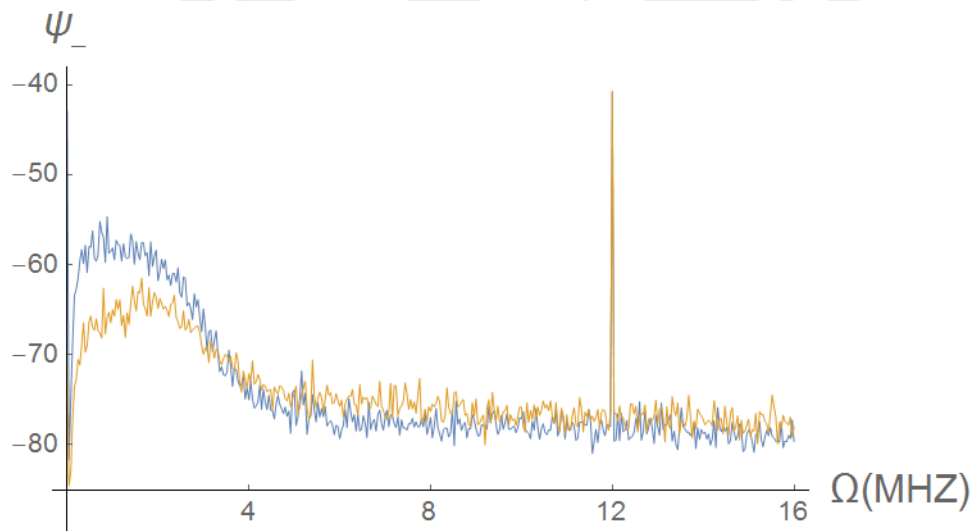


Figure 7.3: Spectrum of the intensity difference (dB) in blue, and the shot noise limit in orange, the important results should be seen after the 4 MHz, before this value the electronic noise influence the measurement.

Finally, Figure 7.4 shows us the difference of the spectra in a range of 5 to 9 MHz. It helps us to get a quantitative picture. There we can see that in the range of 7.4 to 7.8 MHz we obtain the highest compression of noise, reaching a difference of 2.65 dB.

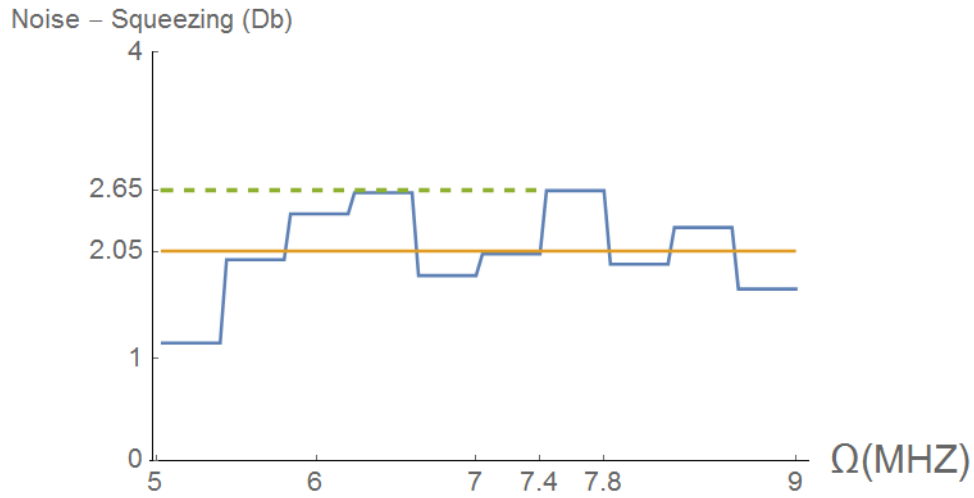


Figure 7.4: Here we can see in blue the difference in spectrums, dashed line is the highest value of the difference, and the orange line is the mean of the difference in the range of 5 to 9 Mhz.

7.4 Conclusions

Both Figure 7.3 and 7.4 show that we have obtained a notorious noise compression, which lies under the shot noise limit, using a plane – concave configuration for the OPO cavity and the highly correlated beams generated by the KTP crystal. This is a notorious prove that we have gotten the squeezed state wanted.

Chapter 8

Injected Optical Parametric Oscillator

The present sections are strongly related to the work done by B. Coutinho et al. [1]. We are interested in the study of the symmetry of the OAM in an injected OPO. Here we are not interested in working above the threshold of the OPO, because for this experiment we have a seed beam. This means that there will be an initial intensity for the signal field carrying OAM. However, the pump field will still operate in the fundamental mode. The dynamical equations now should take into account OAM for the injected OPO. They read

$$\begin{aligned}\frac{da_p}{dt} &= -(\gamma_p + i\Delta_p)a_p - g(a^s_+a^i_- + a^s_-a^i_+) + \eta_p a^p_{in} \\ \frac{da^s_+}{dt} &= -(\gamma + i\Delta)a^s_+ + g(a^{i*}_-a_p) + \eta_s a^{s,in}_+ \\ \frac{da^s_-}{dt} &= -(\gamma + i\Delta)a^s_- + g(a^{i*}_+a_p) + \eta_s a^{s,in}_- \\ \frac{da^i_+}{dt} &= -(\gamma + i\Delta)a^i_+ + g(a^{s*}_-a_p) \\ \frac{da^i_-}{dt} &= -(\gamma + i\Delta)a^i_- + g(a^{s*}_+a_p)\end{aligned}\tag{8.1}$$

Most of the parameters were already explained for the OPO in the previous chapter. The new feature of these equations are the lower indexes “+” and “-” they are referred to LaguerreGaussian modes with topological

charges +1 and -1. This is required because we are going to describe the OAM states in the next way

$$|\theta, \phi\rangle = \cos \theta |LG\rangle_{+1} + e^{i\phi} \sin \theta |LG\rangle_{-1} \quad (8.2)$$

The θ is the polar angle, while ϕ is the azimuthal angle, it describes the states in the OAM sphere discussed previously (with the Laguerre-Gaussian +1 at north pole, and the -1 in the south), so a field will be represented by its intensity $I_j = (a_-^j)^2 + (a_+^j)^2$ and the corresponding spinor $|\theta, \phi\rangle_j$

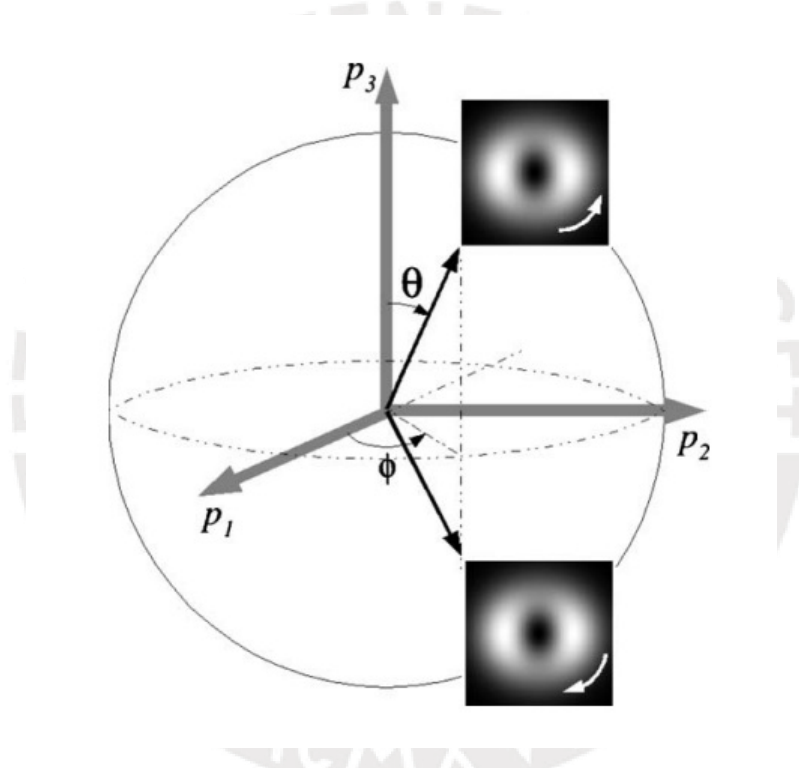


Figure 8.1: Here the OAM sphere shows the parametrization used in equation 8.2, the north pole has the LG mode +1 while the south pole LG -1

8.1 Free Running OPO

Let us start by reminding some already known results using the following simplification:

$$\begin{aligned} a^{s,in}_{\pm} &= 0 \\ \Delta &= \Delta_p = 0 \end{aligned} \quad (8.3)$$

Of course, with it, we are basically in the OPO case where only the pump field is applied to the cavity. However, we should recall that now the resonant case is not so trivial, because we are dealing with a fundamental pump mode and first order modes in the signal and idler fields. As was mentioned before, the resonant length for modes of different order will not match. These conditions can only be achieved changing the temperature of the crystal and playing with the alignment of the crystal.

Let us investigate what new features equations 8.1 bring us. We still want to check the steady solution. It gives

$$\begin{aligned} (a^s_+)^2 &= (a^i_-)^2 \\ (a^s_-)^2 &= (a^i_+)^2 \end{aligned} \quad (8.4)$$

The values of each component are not fixed. However, the total intensity for the idler and signal fields must be the same. Taking again the consideration of $\phi_{p,in} = 0$, which means that all the other fields will have as reference of phase the pump initial field, this leads us to

$$\begin{aligned} \phi^p &= 0 \\ \phi^s_+ + \phi^i_- &= 0 \\ \phi^s_- + \phi^i_+ &= 0 \end{aligned} \quad (8.5)$$

Again we do not have a defined phase difference, and the intensities are:

$$\begin{aligned} I_p &= \left(\frac{\gamma}{g}\right)^2 \\ I &= |a^j_-|^2 + |a^j_+|^2 = \frac{\gamma_p}{g} \left(\frac{\eta_p a^{p,in}}{\gamma_p} - \frac{\gamma}{g} \right) \quad \text{With } j=s,i \end{aligned} \quad (8.6)$$

These results of course were discussed in the OPO section, but this new treatment help us to analyze the OAM aspect, if we now check the resulting amplitudes of the fields for the signal and idler

$$\begin{aligned}
a_+^s &= \sqrt{I} \cos \frac{\theta}{2} e^{i\phi^s_+} \\
a_-^s &= \sqrt{I} \sin \frac{\theta}{2} e^{i\phi^s_-} \\
a_+^i &= \sqrt{I} \sin \frac{\theta}{2} e^{i\phi^i_+} \\
a_-^i &= \sqrt{I} \cos \frac{\theta}{2} e^{i\phi^i_-}
\end{aligned} \tag{8.7}$$

It is helpful for the work done to write the phase difference in 8.5 as $\phi_-^s - \phi_+^s = \phi_-^i - \phi_+^i = \phi$, because in this way both states in the spinor notation can be described as:

$$\begin{aligned}
|\psi_s\rangle &= |\theta, \phi\rangle \\
|\psi_i\rangle &= |\pi - \theta, \phi\rangle
\end{aligned} \tag{8.8}$$

As a first approach, using 8.4 we see some new features, because equation 8.8 tells us that even when the position of signal and idler in the OAM sphere is not totally defined, they show a symmetry, with respect to the polar angle. It does not matter the position of the signal field (seed beam) in the sphere, the idler field will be in the symmetric position with respect to the equator.

8.2 Injected OPO Dynamics

Now let us see the consequences of the injection of a seed beam as the signal field. In order to be general enough, let us consider the generalized first order OAM state $|\theta_0, \phi_0\rangle$ with

$$\begin{aligned}
a_+^{s,in} &= \sqrt{I^{in}_s} \cos \frac{\theta_0}{2} \\
a_-^{s,in} &= \sqrt{I^{in}_s} \sin \frac{\theta_0}{2} e^{i\phi_0}
\end{aligned} \tag{8.9}$$

In the same way the signal and idler fields can be written like

$$\begin{aligned}
a^s &= \cos \frac{\theta_0}{2} a_+^s + \sin \frac{\theta_0}{2} e^{-i\phi_0} a_-^s \\
a^i &= \sin \frac{\theta_0}{2} e^{i\phi_0} a_+^i + \cos \frac{\theta_0}{2} a_-^i
\end{aligned} \tag{8.10}$$

This will lead us to the same OPO equations written in 6.11 with $a^{i,in} = 0$. Solving these equations we get:

$$\begin{aligned}
a_s &= \frac{\eta_p \gamma \sqrt{I_s^{in}}}{\gamma^2 - g^2 |a_p|^2} \\
a_i &= \frac{a_p \eta_p \gamma \sqrt{I_s^{in}}}{\gamma^2 - g^2 |a_p|^2}
\end{aligned} \tag{8.11}$$

This expression constitutes an important practical test to check the amplification process. First of all, we can see that if we calculate the intensities there is no threshold of oscillation, the only condition for amplification of the idler field is that $I_s^{in} \neq 0$. This is a very convenient condition, because we do not need a high power laser to see the phenomenon taking place, which sometimes is a very hard difficulty to solve in OPO experiments.

Finally the signal and idler fields as functions of the Laguerre-Gaussian modes are:

$$\begin{aligned}
|\psi_s\rangle &= \frac{\eta_p \gamma \sqrt{I_s^{in}}}{\gamma^2 - g^2 |a_p|^2} \times [\cos \frac{\theta_0}{2} |LG\rangle_{+1} + e^{i\phi_0} \sin \frac{\theta_0}{2} |LG\rangle_{-1}] \\
|\psi_i\rangle &= \frac{a_p \eta_p \gamma \sqrt{I_s^{in}}}{\gamma^2 - g^2 |a_p|^2} e^{-i\phi_0} \times [\sin \frac{\theta_0}{2} |LG\rangle_{+1} + e^{i\phi_0} \cos \frac{\theta_0}{2} |LG\rangle_{-1}]
\end{aligned} \tag{8.12}$$

Now it is clear that the symmetry with respect to the equator still holds in this case, and this was part of the experimental proposal done by the UFF's quantum optics team, which I had the pleasure to work with for some months.

8.3 Experimental Proposal

In the UFF we had an operating OPO cavity, which was used for squeezing measurements, as described before. This same cavity was the one used to show the OAM symmetry in great fashion.

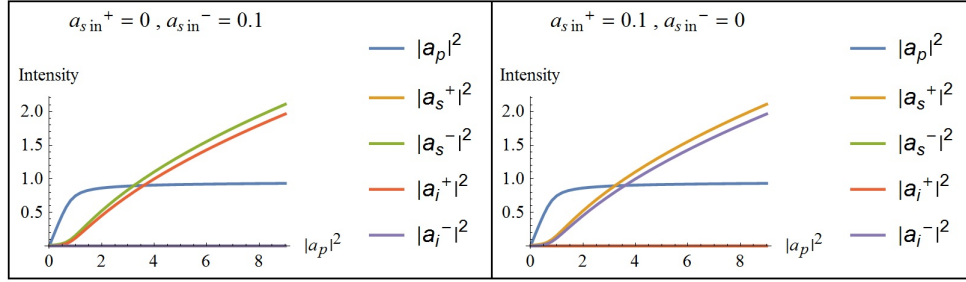


Figure 8.2: These graphics are numerical simulations of the equations 8.1 , here we can see that in the left side when we insert the signal field with topological charge -1 we obtain amplification in the idler field with the topological charge +1. While in the right side ,inserting the signal field +1 we obtain the amplification in the idler field with -1. These simulations reflect the symmetry discussed in this chapter

The experimental parameters were mostly the same for the squeezing measurements, but two more elements were added, as it is shown in the experimental set up.

The first one is the Mode Preparation Stage (MP Stage). This was designed to the preparation of a generalized qubit in our OAM 2 level space. It was done using the infrared (1024 nm.) horizontal polarized light coming from the diabolo laser (before used to calibrate the shot noise), referred in the Figure 28 as “b1”. It passes through the LG-mask, which is an holographic mask that created the Laguerre-Gaussian with topological charge +1 in its first diffraction order. Then it goes through the first Half Wave Plate (HWP) that changes the polarization, and it enters to a Mach-Zehnder type interferometer. As shown in the setup, one arm of the interferometer has an extra mirror. This is used to change the sign of the Laguerre-Gaussian mode [21] . In that way, at the output of the interferometer we got a superposition of the two Laguerre – Gaussian modes (+1 and -1) . The relative phase between them is achieved with the PZT mounted on a mirror of one of the arms. At the end of the interferometer, a HWP and a PBS are put to balance the intensities of both arms.

The second difference with the previous squeezing measurement is the Tilted Lens stage. The lens is put after the OPO cavity and affects the signal and idler beams by the process that was already explained in the experimental methods. Once they are transformed to their corresponding

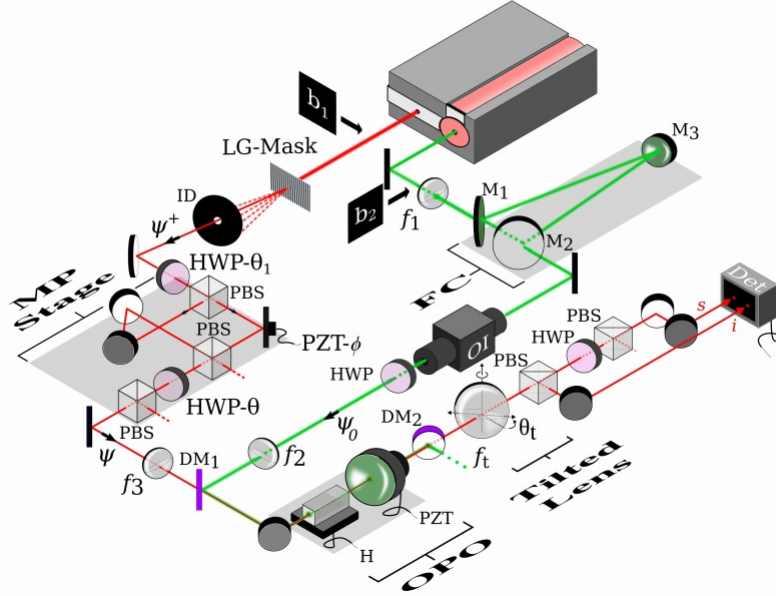


Figure 8.3: Optical Parametric Amplifier Setup

Hermite-Gaussian modes, a PBS separates both beams due to their orthogonal polarizations. Finally, they are recorded in a CCD camera.

We need to mention that mode matching conditions are achieved using a set of lenses for both beams (“b1” and “b2”). They are coupled by a Dichroic Mirror (DM1). It works as a mirror for the green light (532 nm) while it transmits the infrared. The heating control system helped us to control the simultaneous resonance of the seed and the pump in the OPO cavity.

8.4 Experimental Results

While I was working at UFF, we could realize the experimental proposal. However, we had not the versatility that the Mode Preparation stage gives presently, so we made the experiment only with the holographic mask. In that way, we only checked the case of topological charge +1 for the seed beam (in consequence, -1 for the idler field) which corresponds to points 1 and 9 in Figure 8.5.

Using the mode preparation stage it is possible to follow the trajectory

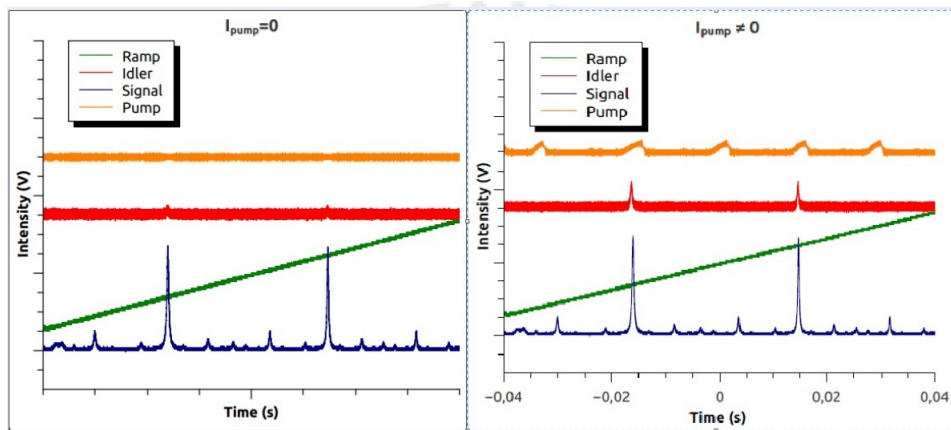


Figure 8.4: This were experimental graphics seen in the oscilloscope , the green one shows the “Ramp” which is the movement of the PZT mounted on the mirror of the OPO cavity, the blue line is the signal field, yellow for the pump and red for the idler. This was the practical test that let us know that the amplification is going on, in the left side the graphic shows no pump intensity, in consequence there is not idler field according to equation 8.12 , once we add pump intensity as is shown in the graphic of the right side inmediately the idler field appears, which was the objective of the whole project.

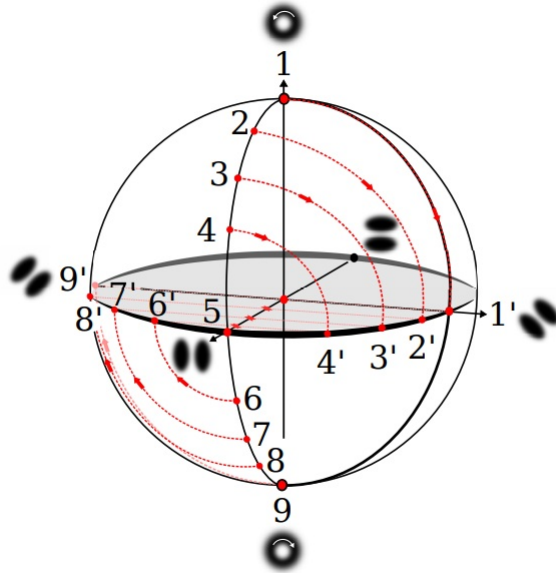


Figure 8.5: The initial states for the seed beam are the ones above the equator, from 1 to 5, while the points under the equator correspond to the expected state of the idler field, the prime number are the theoretical projection done by the tilted lens method.

shown in Figure 8.5.

Using the setup of the OPA, it was possible to see both signal and idler before and after the tilted lens easily, the results are shown in Figure 8.6. They show a behavior that was in accordance with the expected one. Now we can compare the inclination of the Hermite Modes with the expected one. Figure 8.7 shows the best fit of the measured points.

8.5 Conclusions

We have shown the symmetry of the OAM in an injected OPO with experimental results that match very good with the theory. The most important result is that we have explored not only the pure cases of topological charge that are well defined (the poles of the OAM sphere) but also more complex superpositions of the OAM space of order 1.

It could be interesting, as a further research along this line, to use a higher

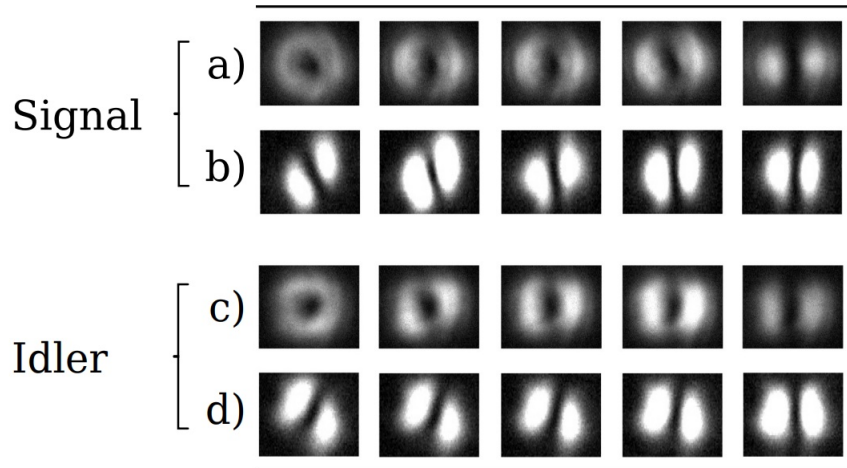


Figure 8.6: Experimental qualitative results , the top row of signal and idler show the intensity distribution of the fields, the lower row shows the beams after the tilted lens transformation.

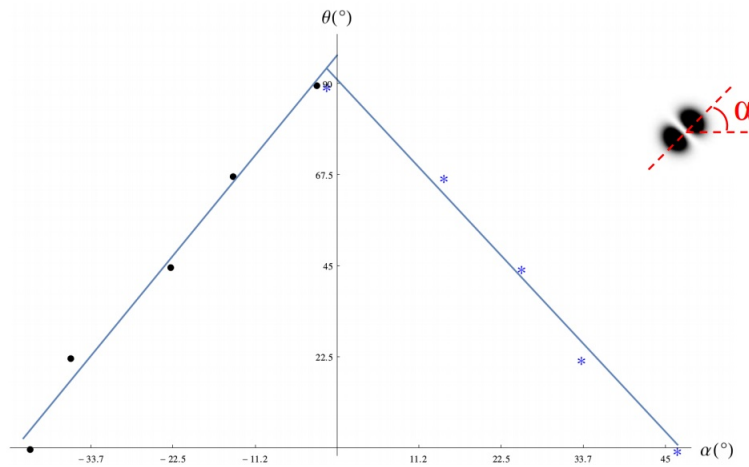


Figure 8.7: These are quantitative results, the angle α is the inclinations of the beams after the tilted lens, while the angle θ is the parameter to describe the original beams in the OAM sphere. The points correspond to the signal beam, while the stars to the idler one.

order beam as a seed and explore its implications.



Chapter 9

Summary and Conclusions

In this thesis we have reviewed important topics from basic electromagnetism, mainly dealing with the paraxial approximation which led us to the discussion of Transverse spatial modes, that contained the nowadays very studied Laguerre-Gaussian beams as well as the Hermite-Gaussian modes. In this work we have also pointed out the analogy between the well known Poincaré Sphere (used for polarization) and the 2-level space expanded in terms of the modes of first order. We have also reviewed the implications of the Orbital Angular Momentum and why they are linked with the Laguerre-Gaussian beams.

Related to the optical cavities/resonators this thesis did a review on the formalism of ABCD law, which is of great importance not only for optical cavities but in the general approach to deal with large sequences of optical devices. The stability criterion and typical losses in optical resonators were also discussed and the frequency of resonance of these cavities were explained on the chapter 3.

Chapter 4 talked about the experimental procedures that were used during the experiments performed, here I contributed to the work with a program that was able to calculate the new intensity values required to measure the waist for the Laguerre-Gaussian modes, it was inspired in the well known definition of the waist in the case of the fundamental (Gaussian) mode, the new method was used to mode-match the beams in the last experiment. Chapter 5 gave a very brief review of the correlations presented in quantum mechanics.

The main experiments reported in this thesis were the measurement of “Squeezing” (Chapter 7) and the “OAM Symmetry” (Chapter 8). The first

experiment was already performed on the UFF some time before I started to work there, so in fact they had an Optical Parametric Oscillator (Chapter 6) already working, since I got to the university we performed a second run of the squeezing experiment, which had a successful result showing a noise compression of 2.65 dB in the range of 7.4 to 7.8 MHz. In this spirit we had interest in pumping the OPO with a Laguerre-Gaussian mode instead of the fundamental mode, however many difficulties arise due to the lack of laser power, but this would still be a very interesting future experimental proposal.

The second experiment followed the proposal done by Coutinho et al. [1] and intended to show the symmetry in the OAM sphere between the twin photons generated inside the OPO cavity in presence of a seed beam which was the one who carried the OAM. The experimental results were very successful and are presented in the last chapter. The seed beam was a superposition of the 2 Laguerre-Gaussian modes of first order corresponding to $l = +1$ and $l = -1$, so it was a general OAM qubit, however future research could move on higher dimensional OAM spaces, and explore its implications in the twin beams generated. As a result of this work there is a paper under development that is going to be presented later on, but at this date it is still being written.

Bibliography

- [1] B Coutinho dos Santos et al. “Phase conjugation and adiabatic mode conversion in a driven optical parametric oscillator with orbital angular momentum”. In: *Physical Review A* 76.5 (2007), p. 053821.
- [2] R Gordon Gould et al. “The LASER, light amplification by stimulated emission of radiation”. In: *The Ann Arbor conference on optical pumping, the University of Michigan*. Vol. 15. 1959, p. 128.
- [3] Max Born and Emil Wolf. *Principles of optics: electromagnetic theory of propagation, interference and diffraction of light*. Elsevier, 2013.
- [4] David L Andrews and Mohamed Babiker. *The angular momentum of light*. Cambridge University Press, 2012.
- [5] Melvin Lax, William H Louisell, and William B McKnight. “From Maxwell to paraxial wave optics”. In: *Physical Review A* 11.4 (1975), p. 1365.
- [6] A. E. Siegman. *Lasers (Vol. 37)*. Mill Valley, CA: University Science Books, 1986.
- [7] FJ Belinfante. “On the current and the density of the electric charge, the energy, the linear momentum and the angular momentum of arbitrary fields”. In: *Physica* 7.5 (1940), pp. 449–474.
- [8] Les Allen et al. “Orbital angular momentum of light and the transformation of Laguerre-Gaussian laser modes”. In: *Physical Review A* 45.11 (1992), p. 8185.
- [9] Marco W Beijersbergen et al. “Astigmatic laser mode converters and transfer of orbital angular momentum”. In: *Optics Communications* 96.1-3 (1993), pp. 123–132.
- [10] Amnon Yariv. *Optical electronics*. Saunders College Publ., 1991.

- [11] D Herriott, H Kogelnik, and R Kompfner. “Off-axis paths in spherical mirror interferometers”. In: *Applied Optics* 3.4 (1964), pp. 523–526.
- [12] Pravin Vaity, J Banerji, and RP Singh. “Measuring the topological charge of an optical vortex by using a tilted convex lens”. In: *Physics letters a* 377.15 (2013), pp. 1154–1156.
- [13] Eric D Black. “An introduction to Pound–Drever–Hall laser frequency stabilization”. In: *American Journal of Physics* 69.1 (2001), pp. 79–87.
- [14] Albert Einstein, Boris Podolsky, and Nathan Rosen. “Can quantum-mechanical description of physical reality be considered complete?” In: *Physical review* 47.10 (1935), p. 777.
- [15] John S Bell. “On the einstein podolsky rosen paradox”. In: *John S Bell On The Foundations Of Quantum Mechanics*. World Scientific, 2001, pp. 7–12.
- [16] John F Clauser et al. “Proposed experiment to test local hidden-variable theories”. In: *Physical review letters* 23.15 (1969), p. 880.
- [17] Robert W Boyd. *Nonlinear optics*. Academic press, 2003.
- [18] T Debuisschert et al. “Type-II continuous-wave optical parametric oscillators: oscillation and frequency-tuning characteristics”. In: *JOSA B* 10.9 (1993), pp. 1668–1680.
- [19] Jun John Sakurai and Eugene D Commins. *Modern quantum mechanics, revised edition*. 1995.
- [20] A Heidmann et al. “Observation of quantum noise reduction on twin laser beams”. In: *Physical review letters* 59.22 (1987), p. 2555.
- [21] Hiroyuki Sasada and Megumi Okamoto. “Transverse-mode beam splitter of a light beam and its application to quantum cryptography”. In: *Physical Review A* 68.1 (2003), p. 012323.